

INVESTIGATIONS ON InSb PLASMONIC DEVICES FOR SENSOR APPLICATIONS AT TERAHERTZ FREQUENCIES

Thesis

Submitted in partial fulfilment of the requirements for the degree of

DOCTOR OF PHILOSOPHY

by

SHOURIE RANJANA J

(Reg.No. 100501PH10F01)



DEPARTMENT OF PHYSICS

NATIONAL INSTITUTE OF TECHNOLOGY KARNATAKA

SURATHKAL, MANGALORE – 575025

JULY 2017

INVESTIGATIONS ON InSb PLASMONIC DEVICES FOR SENSOR APPLICATIONS AT TERAHERTZ FREQUENCIES

Thesis

**Submitted in partial fulfilment of the requirements for the degree of
DOCTOR OF PHILOSOPHY**

by

SHOURIE RANJANA J

(Reg.No. 100501PH10F01)

Research Supervisors

Prof. G. Umesh

Dr. M. N. Satyanarayan



DEPARTMENT OF PHYSICS

NATIONAL INSTITUTE OF TECHNOLOGY KARNATAKA

SURATHKAL, MANGALORE – 575025

JULY 2017

DECLARATION

By the Ph.D. Research Scholar

I hereby declare that the Research Thesis entitled “**INVESTIGATIONS ON InSb PLASMONIC DEVICES FOR SENSOR APPLICATIONS AT TERAHERTZ FREQUENCIES**” which is being submitted to the *National Institute of Technology Karnataka, Surathkal* in partial fulfillment of the requirement for the award of the Degree of *Doctor of Philosophy* in Physics, is a *bonafide report of the research work carried out by me*. The material contained in this Research Thesis has not been submitted to any University or Institute for the award of any degree.

Shourie Ranjana J

Reg: No 100501PH10F01

Department of Physics

Place: NITK Surathkal

Date:

C E R T I F I C A T E

This is to certify that the Research Thesis entitled “**INVESTIGATIONS ON InSb PLASMONIC DEVICES FOR SENSOR APPLICATIONS AT TERAHERTZ FREQUENCIES**” submitted *by Shourie Ranjana J (Reg.No: 100501PH10F01)* as the record of the research work carried out by her, is accepted as the *Research Thesis* submission in partial fulfillment of the requirements for the award of degree of *Doctor of Philosophy*.

Research Guides

G. Umesh

M.N. Satyanarayan

Chariman - DRPC

Acknowledgements

If I am what I am today, it was all due to such unlimited cooperation and encouraging supports that was showered on me day in day out. Hence I stand with a responsibility to express my overflowing sentiments of gratitude.

I express my sincere thanks to my supervisors Prof. G. Umesh and Dr. M. N. Satyanarayan. They had offered their expert guidance and support that were essential to successfully complete my PhD. I was able to gain valuable life experiences from each interaction that I had with each of them. As teachers, they had enabled me to open the book of knowledge and spot out many aspects of my research activities. As human persons, they had offered me constant motivation and guidance. I'm very grateful to each of them for the dedicated support and encouragement they had rendered to me.

I thank the Director, Dean of Academic Affairs, and Dean – Research and Consultancy and the Department of Physics for their supports and guidance given all through my stay at NITK. I gratefully remember and say 'Thank You' for awarding me the full time Institute Research Scholarship.

With a grateful heart, I thank Prof. H.D. Shashikala - Head, Department of Physics and Chairman, Prof. G. K. Shivakumar Department of Physics and Prof. Sripathi Department of Electronics and Communication Engineering, Members of the RPAC Committee. They had spent their precious time, attending my seminars, evaluating my work and provided me valuable suggestions during each of those discussions that I had with them.

I thank Prof. Kasturi V. Bangera, Prof. N.K. Udayashankar, Dr. H.S. Nagaraja, Dr. Ajith K.M for offering me moral support and best wishes.

I express my thanks to Dr. K.B. Manjunath, Dr. Vikas M. Shelar, Mr. Hidayath Ulla, Ms. Jean Maria Fernandes, Mr. Ravindra Kiran, Mr. Nimith, Mr. Achutha, Mr. Mahesh for their cooperation and support. I thank Mr. Shashidhara for extending his support during my initial experimental works at NITK.

Acknowledgements

I extend my sincere thanks Mr.M.Chandranath, Mr.Sheshappa Naik, Mrs. Sarita Shetty, Ms. Usha, Mrs. Ashalatha, Mr. Dhanaraj and Mrs.Mohini Department of Physics for administrative assistance.

My sincere and heartfelt thanks to Dr S.S. Prabhu, Department of Condensed Matter Physics, TIFR – Mumbai for his generous support, immense guidance in helping me to use his lab facility. I as well thank his research students, Dr. Reddy, Mr. Harshad, Mr. Prathamesh and Mr. Abishek for being generous and supportive in helping me carry out my experiments.

I offer my sincere thanks to Dr. Nageshwari IITBNF, IITB Mumbai for offering her full support during my INUP Projects. I thank Mr. Rajaram and Mr. Aravind who had helped me to fabricate the devices by Laser Micromachining in Mumbai.

I say a very special thanks to Mr. Piyush Bhatt who had assisted me in a very special manner especially when I had to work at IITB and TIFR – Mumbai. I make a special note of recognition for valuable suggestions and supports Mr. Piyush Bhatt had lavishly showered and made my research efforts effective.

I thank Mr. Manjunath, Government tools center Baikambady, Mangalore, for precisely fabricating mould for making pellets.

I express my sincere gratitude to Dr. Anandhan Srinivasan, Department of Metallurgical and Materials Engineering, NITK Surathkal and his Research Student Ms. Akshatha Patil for allowing me to use their lab facility to make pellets and providing me with polymer samples.

I thank Dr. Prasanna B. D. Department of Chemical Engineering and Dr. Nagavel B. Department of Electronics and Communication Engineering, NITK Surathkal for fruitful discussions and suggestions.

I whole heartedly thank Ms. Pooja Nanda, Department of Chemical Engineering NITK Surathkal and Mr. Hemant Department of Bioengineering and bioscience IITB – Mumbai

Acknowledgements

and Dr. Rajeev P. Sha NIDAN Pathology Laboratories Thane, Mumbai for generously providing me protein samples and serum samples for device testing.

I thank Editors and Reviewers of MRS, IOP Science, Springer and IEEE- IRMMW for reviewing my research Papers; giving me valuable suggestions; and improving the quality of my publication in their respective journals.

Dr. Beulah Rajkumar was ever an inspiration and guidance from the year that I had joined the Lady Doak College for my undergraduate studies. It was her guidance and encouragement that had opened the scope to the outside world and helped me to do my PhD. Hence, I thank her and pray the Almighty to bless her abundantly.

I proudly acclaim that my family stands as the root and stem of my PhD Tree. They had nurtured and watered it. They had taken care of all my needs and stood by my side in all my difficulties. I bow my head in front of my family members and seek their blessing.

My father Mr. A. Jebamalaidass, mother Mrs. A Maria Madalene, brother Mr. J. Rejoice Raja, sister in law Mrs. G.S. Bhuvaneswari and my sweet niece Ms. Judith Anselina.

Finally, I offer my prayers of thanksgiving to Almighty God who had guided my steps all through those years of my PhD Studies. I recognize his continued presence in my entire endeavour that would enable me to know more, to do moral, and to be more fully alive all through my life time.

SHOURIE RANJANA J.

ABSTRACT

Rapid advances in the field of Plasmonics over the last two decades have led to several practical nano-photonic devices and were largely confined to devices utilizing visible light. Recently, there has been growing interest in plasmonic devices operating at terahertz (THz) frequencies. The interest arose due to its potential applications in detecting minute quantities of certain materials by employing the techniques of THz spectroscopy. Many materials show significant absorption of energy in the THz frequency range, thus enabling their detection by transmission spectroscopy. Further, the fabrication of efficient sources and detectors at THz frequencies has led to development of the technique of THz Time – Domain Spectroscopy (THz-TDS), which has been employed to characterize devices such as THz waveguides, antennas, resonators and filters. Developments in THz devices have attracted considerable attention on THz sensing in the field of biochemistry and medicine. In the effort to develop a highly promising and sensitive THz chemical sensor, this work focuses on experimentally and theoretically investigating the transmission characteristics and hence, the sensing capabilities, of a Semiconductor–Insulator–Semiconductor (SIS) THz waveguide device with stubs. The stubs function as resonant cavities and the device itself functions as a narrow band filter. The devices were made using intrinsic Indium Antimonide (InSb), which is a promising material for THz plasmonics. The resonant transmission characteristics of the device at THz frequencies are exploited for sensing applications. The transmission characteristics of the waveguide device were simulated using finite element method techniques for various sizes of waveguide width and stub length. The waveguide devices were fabricated by laser micromachining and their transmission characteristics were measured by THz-TDS. The experimental results are consistent with the simulation results. The stubs of the device were loaded with Bovine Serum Albumin (BSA) protein molecules and polystyrene dissolved in toluene. Significant change in the THz transmission and absorption coefficient was observed for different concentrations of BSA and polystyrene. Consequent change in the refractive index in the stubs alters the transmitted signal intensity. Results show that, a change in concentration of material loaded in the stub even by 1mol/L, leads to measurable change in the transmission coefficient of the device. Thus, InSb plasmonic waveguide device operating at THz frequencies shows promising potential as a good material sensor.

Keyword: Terahertz radiation, THz- TDS, Waveguide, Plasmonics, Resonator, Sensor.

CONTENTS

CHAPTER 1	Page No
Introduction	
1.1	Theoretical Principles of Plasmonics
1.1.1	Fundamentals of Surface Plasmon..... 3
1.1.2	Dielectric Constant of metals..... 4
1.1.3	SPP propagation in metal dielectric interface..... 6
1.1.4	SPP propagation in 3-layer metal insulator metal (MIM) device. 10
1.2	THz Time domain spectroscopy..... 13
1.3	Literature Review
1.3.1	Surface Plasmons..... 15
1.3.2	Terahertz waveguide devices..... 17
1.4	Scope and Objectives of the thesis work..... 19
CHAPTER 2	
Modelling of InSb Plasmonic THz Waveguide	
2.1	Introduction..... 23
2.2	Importance of InSb in the THz frequency regime..... 24
2.3	Surface Plasmon Modes in InSb Waveguide..... 25
2.4	Effective Index Method Analysis of THz InSb Waveguide..... 27
2.5	Conclusions..... 30
CHAPTER 3	
Transmission Characteristics of the InSb Plasmonic Device	
3.1	Introduction..... 32
3.2	InSb THz plasmonic waveguide with stubs

3.2.1	Device Configuration.....	33
3.2.2	Transmission Characteristics.....	34
3.3	Transmission line model for the device.....	36
3.4	InSb Plasmonic device with two pairs of stubs.....	39
3.5	Conclusions.....	43
 CHAPTER 4		
Fabrication and Characterization of InSb THz Plasmonic Waveguide Device		
4.1	Introduction.....	45
4.2	Fabrication and Characterization.....	46
4.3	Conclusions.....	52
 CHAPTER 5		
InSb waveguide as material sensor		
5.1	Introduction.....	53
5.2	Bovine Serum Albumin.....	55
5.3	Polystyrene Dissolved In Toluene.....	56
5.4	Conclusions.....	59
 CHAPTER 6		
Summary and Conclusions		60
6.1	THz InSb waveguide device with stub as resonant structure.....	60
6.2	THz InSb waveguide device as material sensor.....	61
6.3	Scope for future work.....	62
	References.....	63
	List of Publications.....	70
	Curriculum vitae.....	71

List of Abbreviations

THz	Terahertz
InSb	Indium Antimonide
THz- TDS	Terahertz-Time domain Spectroscopy
SPP	Surface Plasmon Polaritons
PEC	Perfect Electric Conductor
BSA	Bovine Serum Albumin
PS	Polystyrene
MIM	Metal- Insulator- Metal
SIS	Semiconductor-Insulator-Semiconductor
TM	Transverse Magnetic
TE	Transverse electric
ZnTe	Zinc Telluride
PPWG	Parallel Plate Waveguide
EIT	Electromagnetically Induced Transparency
RIU	Refractive Index Unit
EIM	Effective Index Method
FWHM	Full Width half Maximum
FFT	Fast Fourier Transform
fs	femtosecond
mg	milligram

Nomenclature

ϵ'	Real part of permittivity
ϵ''	Imaginary part of permittivity
ϵ_m	Complex permittivity of metal
ϵ_d	Permittivity of dielectric
n_{eff}	Effective refractive index
α_{eff}	Effective absorption coefficient
ω	Angular frequency
λ	Wavelength
ω_p	Plasma Frequency
β	Propagation Constant
N	Carrier concentration
m^*	Effective mass
f_c	Cut-off frequency
f_R	Resonant Frequency
Z_L	Load Impedance
T	Transmission coefficient

CHAPTER 1

INTRODUCTION

Over the past 50 years our world has been rapidly evolving into a society dominated by smart gadgets in every facet of our life. This evolution has been driven largely by advances in electronics and photonics. A hallmark of the technological development has been the continuing miniaturization of electronic devices which has now reached the sub 14nm level. The electronic chips fabricated currently have billions of such electronic devices leading to highly efficient electronic systems. At such small sizes the performance of the devices is strongly governed by the laws of Quantum Physics which may ultimately put a limit on further miniaturization. On the other hand photonic devices are traditionally macro sized in comparison. This is simply because propagation of light is understood in terms of the diffraction theory of light formulated by Gustav Kirchhoff in late 19th century. Significant miniaturization in photonic devices was achieved after the invention of optical fibres around 1970. However, the device size still had to comply with Kirchhoff's diffraction theory of light. An equally important aspect of photonics is the frequency range of the radiation being employed for different applications. Past research has led to excellent exploitation of radiation in the radio frequency and microwave domains, extending from a few kilohertz to about 200 gigahertz. Similar progress was achieved in the optical domain spanning from Far-Infrared (FIR: wavelength below about 30 μ m) to Extreme-Ultra-Violet (XUV: wavelength upto 100nm). Exciting progress has also been achieved recently at X-Ray wavelength, the domain of X-Ray Optics, wherein devices such as efficient mirrors and focusing devices have been developed. Since the mid-1980s, there has been growing interest in creating devices operating in the terahertz (THz) frequency domain ranging from 0.1 to 10 THz (wavelength range: 30 μ m to 3mm) leading to the emergence of the new field of "Terahertz Science and Technology". These advances were triggered by the development of reliable sources and detectors at THz frequencies in early 1990s. Further, the possibility of using THz radiation for detecting plastic-explosives gave a tremendous boost to research in this field. This interest has now expanded to include study of many other materials using the techniques of Terahertz Spectroscopy.

It is but natural that many concepts and strategies developed for the microwave domain and the optical domain have influenced the researches in THz domain. Thus, there is interest in not only free-space optics but also guided wave optics. However, progress has been rather limited in the domain of Guided Wave Devices at THz frequencies. The difficulties arise mainly due to the absorption and dispersion properties of different materials at such frequencies. Propagation of radiation in waveguides is subject to attenuation and dispersion of the travelling wave, which in turn strongly depends on the dielectric properties possessed by the materials used for fabricating the waveguides. Further, as mentioned above, the device sizes have to be several times the wavelength of the radiation, i.e. larger than about $50\mu\text{m}$. Thus, miniaturization of optical devices is not feasible if they are made using purely dielectric materials, since their dielectric constants are real positive numbers, assuming that the absorption of radiation is negligible.

Recent research, carried out over the last two decades, has led to the exciting possibility of fabricating low loss optical waveguide devices of sub-wavelength dimensions by exploiting the optical properties of metals at optical frequencies and semiconductors at THz frequencies. The striking feature of such devices is that they are essentially surface wave devices consisting of a patterned metal or semiconductor thin film deposited on a dielectric substrate. The fact that metals or semiconductors can exhibit negative dielectric constant below a certain frequency is the crucial factor responsible for this. More explicitly, negative dielectric constant arises due to the coupling of the electromagnetic radiation with the free electron gas in the metal or semiconductor film. Such coupling excites propagating surface waves even if the propagation channel has a width much less than the free space wavelength of the radiation. The propagation characteristics of the waveguide device can be analyzed using the Maxwell Equations taking into account the dynamics of the free electron gas which manifests itself in the form of Plasma Waves within the metal/semiconductor film. Investigations on standard waveguide configurations have revealed that these devices are quite lossy and, hence, the waves propagate over a very short length. Consequently, any plasmonic device operating at THz frequencies would be a miniature device suitable for signal processing and near field optics.

One of the interesting applications of plasmonic devices is as a sensor for various materials. Loading a plasmonic device with the material to be detected results in

alterations in the propagation characteristics of the electromagnetic wave being guided in the device and accurate measurement of the changes enables one to identify the material. For this purpose one may incorporate one or more stubs in the waveguide section which, in turn, makes the device a resonant structure. Two of the parameters suitable for material sensing are the transmission coefficient and resonance frequency shift. The fact that the refractive index of any material is generally a complex number implies that, when the material is loaded into a resonant device, both the resonant frequency and the reflection coefficient will be altered. The big advantage with a resonant device is that such alterations can result from a minute amount of the material. Thus, one expects to achieve high sensitivity for the detection of materials, especially by measurement of frequency shifts. The choice of terahertz radiation for our work was dictated by the fact that such radiation excites vibrational and rotational degrees of freedom of large molecules which might yield unique identifiable signature for the molecule. One, therefore, hopes to be able to design good quality sensors for organic and bio molecules. This possibility is the main motivation for our research work.

In the present work we have investigated in detail the propagation characteristics of a waveguide device having two stubs in the middle part of the device. Such devices were fabricated using intrinsic Indium Antimonide (InSb) pellet. Prior to fabricating the device, a detailed simulation of the wave guiding characteristics of the InSb devices, with and without the stubs, was investigated by simulation using COMSOL Multiphysics and Ansoft HFSS. On the basis of these preliminary studies, the device dimensions were chosen. We carried out experimental studies on two specific materials to demonstrate the sensor application. Due to limitations of the laboratory facilities, our investigations are based only on the measurement of the changes in the transmission characteristics of the device. We were able to detect the presence of a few micro-litres of a solution containing the sample material.

1.1 THEORETICAL PRINCIPLES OF PLASMONICS

1.1.1 Fundamentals of Surface Plasmon

Devices made using metals, semiconductors and dielectrics are known to guide electromagnetic (EM) waves, in the interfaces, called surface plasmon polariton (SPP) modes (Barnes et al. 2003). These are electromagnetic waves coupled to collective

plasma oscillations of the free electron gas in metals and semiconductors. Such waves can be generated close to the plasma frequency associated with the free electrons by either a beam of light or an electron beam incident on the interface. The electric field pattern of such waves is shown in figure 1.1. It is seen that the surface plasmon (SP) propagates along the interface and the wave field is evanescent perpendicular to the interface. In other words, the fields decay exponentially in the metal as well as the dielectric regions. The penetration of the field into the metal is much smaller than that into the dielectric due to the screening effect of the free charge carriers (Stefan A Maier. 2006).

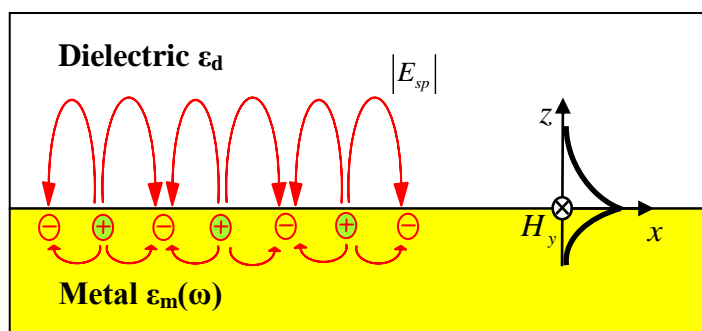


Figure 1.1: Schematic of electric field lines associated with charge oscillations and the variation of the field transverse to the metal/dielectric interface.

1.1.2 Dielectric Constant of Metals

The basic theory behind SPPs can be understood in the classical framework based on Maxwell's equation and also on the dispersive properties of metal. The dielectric permittivity of a material relates the electric displacement vector \vec{D} , and the electric field \vec{E} as a function of frequency of the electromagnetic field. The dielectric properties of metals can be explained by a plasma model, where a gas of free electrons of number density N moves in a fixed background of positive ion cores. This is called as the **Drude mode** (Paul Drude 1900).

A simple equation for the motion of electrons in plasma subjected to an oscillating electric field \vec{E} and damping force γ is given by,

$$m\ddot{x} + m\gamma\dot{x} = -e\vec{E} \quad (1.1)$$

If we assume harmonic time dependence $E(t) = E_0 e^{-i\omega t}$ for the driving field, the solution of this equation describing the oscillation of the electron is given by $x(t) = x_0 e^{-i\omega t}$.

Substituting this solution in Eq. 1.1 we get,

$$x(t) = \frac{e}{m(\omega^2 + i\gamma\omega)} E(t) \quad (1.2)$$

The displacement of the electrons, in the positive ionic background, leads to macroscopic polarization $P = -nex$ given by,

$$P = -\frac{Ne^2}{m(\omega^2 + i\gamma\omega)} \vec{E} \quad (1.3)$$

Inserting this expression for P into $D = \varepsilon_0 E + P$ yields,

$$D = \varepsilon_0 \left(1 - \frac{\omega_p^2}{\omega^2 + i\gamma\omega} \right) \vec{E} \quad (1.4)$$

From the linear relationship between \vec{D} and \vec{E} , the relative dielectric constant of the metal is given by

$$\varepsilon(\omega) = 1 - \frac{\omega_p^2}{\omega^2 + i\gamma\omega} \quad (1.5)$$

where $\omega_p^2 = \frac{Ne^2}{\varepsilon_0 m_e}$ is the electron plasma frequency, N is the number density of electrons,

m_e is the effective mass of the electron in the material, and $\gamma = 1/\tau$ is the characteristic electron-ion collision frequency, τ is the relaxation time typically on the order of 10^{-14} seconds at room temperature. Typically, plasma frequency for metals is in the ultraviolet (UV) range. It may be noted that the dielectric function is complex in general, indicating that EM fields propagating in metals get attenuated. The real and imaginary components of this complex dielectric function $\varepsilon(\omega) = \varepsilon_1(\omega) + i\varepsilon_2(\omega)$ are given by

$$\varepsilon_1(\omega) = 1 - \frac{\omega_p^2 \tau^2}{1 + \omega^2 \tau^2} \quad (1.6)$$

$$\varepsilon_2(\omega) = 1 - \frac{\omega_p^2 \tau}{\omega(1 + \omega^2 \tau^2)} \quad (1.7)$$

where, the real part of the dielectric function determines the wavelength of the EM wave and the imaginary part determines the amount of absorption inside the medium.

The above description of dielectric function is valid for an ideal metal where $\epsilon \rightarrow 1$ at $\omega \gg \omega_p$. However, for real metals (e.g. Au, Ag, Cu) at optical frequencies or semiconductor at THz frequencies, for $\omega > \omega_p$ there exists residual polarization due to the positive background of the ion cores given by $\vec{P}_\infty = \epsilon_0 (\epsilon_\infty - 1) \vec{E}$ ($1 \leq \epsilon_\infty \leq 10$).

Therefore, the dielectric constant is expressed as

$$\epsilon(\omega) = \epsilon_\infty - \frac{\omega_p^2}{\omega^2 + i\gamma\omega} \quad (1.8)$$

where, ϵ_∞ is the high frequency dielectric constant.

1.1.3. SPP propagation in metal dielectric interface

In order to understand the propagation of SPPs, Maxwell's equations are applied to the plane interface between a conductor and a dielectric:

$$\nabla \cdot \vec{D} = \rho_{free} \quad (1.9)$$

$$\nabla \cdot \vec{B} = 0 \quad (1.10)$$

$$\nabla \times \vec{E} = -\frac{\partial \vec{B}}{\partial t} \quad (1.11)$$

$$\nabla \times \vec{H} = \vec{J}_{free} + \frac{\partial \vec{D}}{\partial t} \quad (1.12)$$

These equations, link the four macroscopic fields \vec{D} (the dielectric displacement), \vec{E} (the electric field), \vec{H} (the magnetic field), and \vec{B} (the magnetic induction or magnetic flux density), with the external charge and current densities ρ_{free} and \vec{J}_{free} . The total charge and current densities are given by $\rho_{tot} = \rho_{free} + \rho_{bound}$ and $\vec{J}_{tot} = \vec{J}_{free} + \vec{J}_{bound}$.

Figure 1.2 shows a planar structure consisting of a metal half-space, defined by $Z < 0$, with complex dielectric constant ϵ_m , and a dielectric half-space, defined by $Z > 0$, with

positive real dielectric constant ϵ_d . The metal-dielectric interface is the X-Z plane located at $Z = 0$. Such structures can support electromagnetic surface waves, called Surface Plasmon Polariton (SPP) waves. We consider the waves to propagate along X-axis and decay exponentially along the Z-axis. The fields have no variation along the Y-axis.

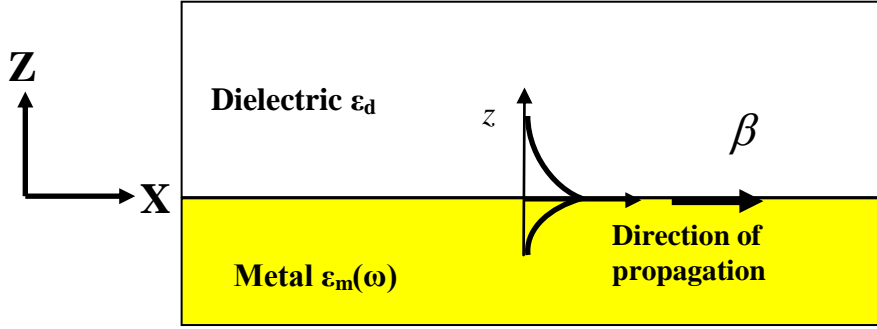


Figure 1.2: Geometry of the Planar Metal-Dielectric structure showing the lower half-space $Z < 0$ as a metal, with a complex dielectric constant ϵ_m , and the upper half-space $Z > 0$ as a dielectric with positive real dielectric ϵ_d . The SPP wave propagates along the X-axis and is shown to decay exponentially along the Z-axis.

Maxwell's equations can be combined to form the wave equation, which may be expressed as

$$\nabla^2 \vec{E} - \frac{\epsilon}{c^2} \frac{\partial^2 \vec{E}}{\partial t^2} = 0 \quad (1.13)$$

For the planar structure shown in figure 1.2 we may assume that the dielectric constant ϵ depends only on the Z coordinate, i.e. $\epsilon = \epsilon(z)$ and the solution of the wave equation may be written as

$$E(x, y, z) = E(z)e^{i\beta x} e^{-i\omega t} \quad (1.14)$$

where β is the propagation constant of the travelling wave. Substitution of the above expression into the wave equation Eq. 1.13 yields,

$$\frac{\partial^2 \vec{E}}{\partial z^2} + (k_0^2 \epsilon - \beta^2) \vec{E} = 0 \quad (1.15)$$

To analyse the modes supported by the planar structure in detail we substitute Eq. 1.14 into Eq. 1.11 and Eq. 1.12 and obtain the following coupled equations

$$\frac{\partial E_y}{\partial z} = -i\omega\mu_0 H_x \quad (1.16)$$

$$\frac{\partial E_x}{\partial z} - i\beta E_z = i\omega\mu_0 H_y \quad (1.17)$$

$$i\beta E_y = i\omega\mu_0 H_z \quad (1.18)$$

$$\frac{\partial H_y}{\partial z} = -i\omega\varepsilon_0\varepsilon E_x \quad (1.19)$$

$$\frac{\partial H_x}{\partial z} - i\beta H_z = -i\omega\varepsilon_0\varepsilon E_y \quad (1.20)$$

$$i\beta H_y = -i\omega\varepsilon_0\varepsilon E_z \quad (1.21)$$

These coupled equations may be solved to obtain two linearly independent solutions termed as TM-mode and TE-mode having the following field configurations:

- Transverse Magnetic (*TM*) mode (*P* mode) - No magnetic field component in the direction of propagation and the only nonzero components are E_x , H_y , and E_z
- Transverse Electric (*TE*) mode (*S* mode) - No electric field component in the direction of propagation and the only nonzero components are H_x , E_y and H_z

For the TM-polarized SPP propagating at the metal-dielectric interface (Figure. 1.2) the system of governing equations and the wave equation are,

$$E_x = -i \frac{1}{\omega\varepsilon_0\varepsilon} \frac{\partial H_y}{\partial z} \quad (1.22)$$

$$E_z = -\frac{\beta}{\omega\varepsilon_0\varepsilon} H_y \quad (1.23)$$

$$\frac{\partial^2 H_y}{\partial z^2} + (k_0^2\varepsilon - \beta^2)H_y = 0 \quad (1.24)$$

The solutions for the above equations in the dielectric region $Z > 0$ may be written as

$$H_y(z) = A_d e^{i\beta x} e^{-k_d z} \quad (1.25)$$

$$E_x(z) = iA_d \frac{1}{\omega\varepsilon_0\varepsilon_d} k_d e^{i\beta x} e^{-k_d z} \quad (1.26)$$

$$E_z(z) = -A_d \frac{\beta}{\omega \epsilon_0 \epsilon_d} e^{i\beta x} e^{-k_d z} \quad (1.27)$$

In the metallic region $Z < 0$, the solutions become

$$H_y(z) = A_m e^{i\beta x} e^{k_m z} \quad (1.28)$$

$$E_x(z) = -iA_m \frac{\omega \epsilon_0 \epsilon_m}{k_m} e^{i\beta x} e^{k_m z} \quad (1.29)$$

$$E_z(z) = A_m \frac{\beta}{\omega \epsilon_0 \epsilon_m} e^{i\beta x} e^{k_m z} \quad (1.30)$$

These solutions must satisfy the boundary conditions that E_x and H_y be continuous across the interface $Z = 0$. Application of the boundary conditions yields the following relations:

$$A_m = A_d \quad (1.31)$$

$$\frac{k_d}{k_m} = -\frac{\epsilon_d}{\epsilon_m} \quad (1.32)$$

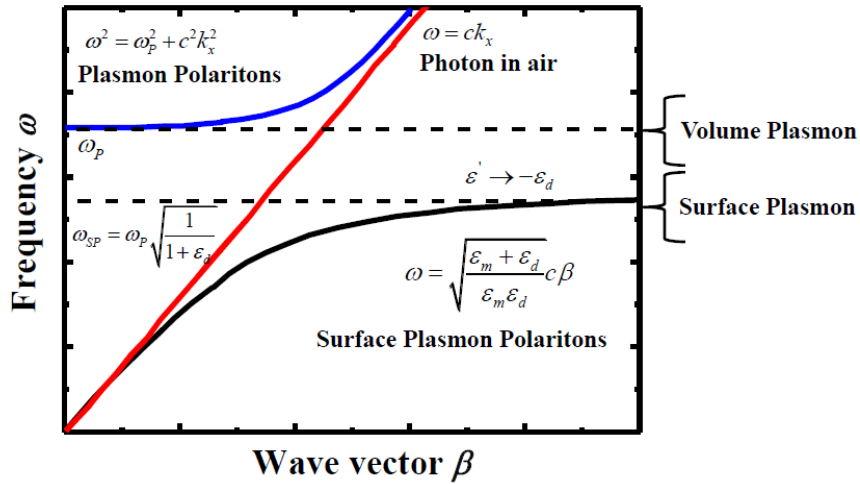


Figure 1.3: Dispersion relation for SPPs propagating along the metal-air interface.

For the TM mode to propagate as a surface wave it must be ensured that $\text{Re}[k_m] < 0$ since practically for any dielectric $\text{Re}[k_d] > 0$. Thus, the surface plasmon waves exist only at interfaces between materials with opposite signs for the real part of their dielectric

permittivity, i.e. a conductor-insulator interface. Further, the expression for H_y has to satisfy Eq.1.24, the wave equation, yielding the dispersion relations:

$$k_m^2 = \beta^2 - k_0^2 \epsilon_m \quad (1.33)$$

$$k_d^2 = \beta^2 - k_0^2 \epsilon_d \quad (1.34)$$

Combining Eq. 1.32 to 1.34, the dispersion relation for SPPs propagating along the interface between the metal and dielectric is given by,

$$\beta = k_0 \sqrt{\frac{\epsilon_m \epsilon_d}{\epsilon_m + \epsilon_d}} \quad (1.35)$$

The dispersion relation for the SPP waves is shown in figure. 1.3. The SPP curve always lies to the right of the light-line, and hence the SPP has a larger wave vector than that for light propagating in an infinite dielectric medium. Thus, Surface plasmons are transverse magnetic (TM) in character and the generation of surface charge requires an electric field normal to the surface. This character also leads to the field component perpendicular to the surface being enhanced near the surface. The field pattern transverse to the interface is seen to be evanescent and, hence, prevents wave power from propagating away from the interface. (Stefan A Maier. 2006).

If we consider the possibility of TE surface wave, using the respective expressions for TE field components from the coupled equation, gives the following boundary condition that H_x and E_y be continuous across the interface $Z = 0$.

$$A_m (k_m + k_d) = 0 \quad (1.36)$$

$$A_m = A_d$$

Since confinement to the surface requires $\text{Re} [k_m] < 0$ and $\text{Re} [k_d] > 0$, this condition is only fulfilled if $A_m = 0$, so that also $A_d = A_m = 0$. Thus, no surface modes exist for TE polarization. Surface plasmon polaritons only exist for TM polarization.

1.1.4. SPP propagation in a 3-layer metal-insulator-metal (MIM) device

The simplest geometry to analyse propagation of SPPs is metal insulator (MI) structure. In order to analysis SPP in a waveguide configuration, we have to consider a multilayer structure consisting of alternating conducting and insulator layers. Each single interface

can support bound SPPs. If the separation between the interfaces is comparable to or smaller than the decay length of the propagating mode the structure supports coupled modes.

We consider a MIM configuration with metallic conducting regions $Z > +a$ and $Z < -a$ having complex dielectric constant ϵ_m , a dielectric region $-a < Z < +a$, with positive dielectric constant ϵ_d , and with the metal-dielectric interface at $Z = +a$ and $Z = -a$ as shown in figure 1.4.

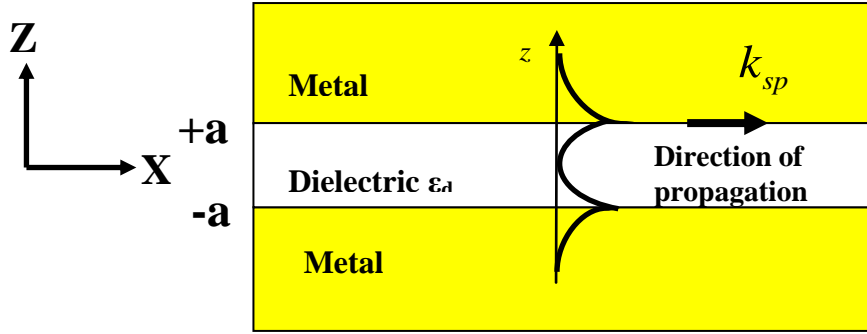


Figure 1.4: Geometry of the Planar Metal-Insulator-Metal structure showing metallic region for $Z > +a$ and $Z < -a$ with a complex dielectric constant ϵ_m and dielectric region for $-a < Z < +a$ with a positive real dielectric constant ϵ_d . The SPP wave propagates along the metal-dielectric interface in the X-direction and is shown to decay exponentially along the Z-axis.

For the 3- layer structure shown in figure 1.4 the field components of the SPP mode propagating along the X-axis at the interfaces at $Z = -a$ and $Z = +a$ are given by,

$$H_y = A e^{i\beta x} e^{-k_m z} \quad (1.37)$$

$$E_x = iA \frac{1}{\omega \epsilon_0 \epsilon_m} k_m e^{i\beta x} e^{-k_m z} \quad (1.38)$$

$$E_z = -A \frac{1}{\omega \epsilon_0 \epsilon_m} e^{i\beta x} e^{-k_m z} \quad (1.39)$$

If the separation (equal to $2a$) between the two interfaces is comparable to the decay length of the wave in the dielectric medium, then the wave solutions in the core region $-a < Z < +a$ correspond to coupled modes and may be expressed as :

$$H_y = Ce^{i\beta x} e^{k_d z} + De^{i\beta x} e^{-k_d z} \quad (1.40)$$

$$E_x = -iC \frac{1}{\omega \varepsilon_0 \varepsilon_d} k_d e^{i\beta x} e^{k_d z} + iD \frac{1}{\omega \varepsilon_0 \varepsilon_d} k_d e^{i\beta x} e^{-k_d z} \quad (1.41)$$

$$E_z = C \frac{\beta}{\omega \varepsilon_0 \varepsilon_d} e^{i\beta x} e^{k_d z} + D \frac{\beta}{\omega \varepsilon_0 \varepsilon_d} e^{i\beta x} e^{-k_d z} \quad (1.42)$$

The requirement of continuity of H_y and E_x across the interfaces leads to

$$Ae^{-k_m a} = Ce^{k_d a} + De^{-k_d a} \quad (1.43)$$

$$\frac{A}{\varepsilon_m} k_m e^{-k_m a} = \frac{C}{\varepsilon_d} k_d e^{k_d a} + \frac{D}{\varepsilon_d} k_d e^{-k_d a} \quad (1.44)$$

Solving the above system of linear coupled equations leads to the dispersion relation or the characteristic equation for the propagating TM SPP mode in the MIM structure.

$$\tanh k_d G = \pm \frac{k_m \varepsilon_d}{k_d \varepsilon_m} \quad (1.45)$$

where, ε_m is the frequency dependent permittivity of metal and ε_d is the dielectric permittivity of the insulator. And the + and - signs indicate the symmetric and anti-symmetric solutions for the propagating TM SPP modes.

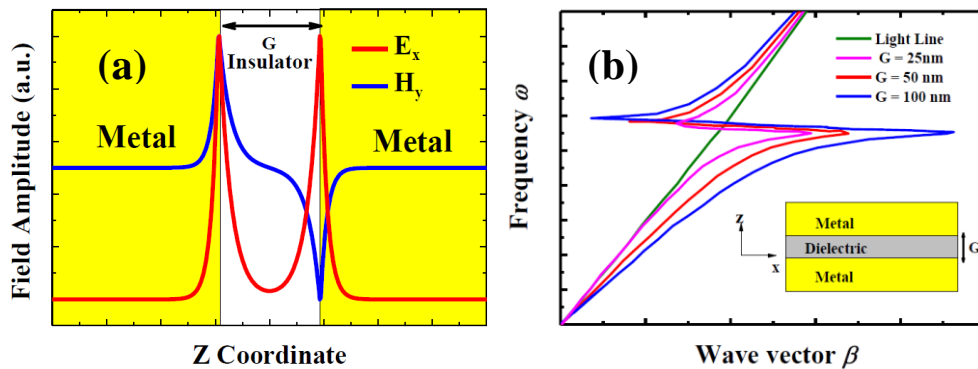


Figure 1.5: (a) E_x and H_y Field component of symmetric TM SPP mode at the MIM waveguide. (b) Dispersion relation of the coupled SPP mode of the MIM waveguide for different waveguide width (G).

Figure 1.5 (a & b) shows the TM SPP field profiles in the MIM waveguide structure and the dispersion relation for the mode. When SPPs are excited at a metal dielectric interface, electrons in the metal create a surface polarization that gives rise to a localized electric field. Metals are lossy and the SPP modes at the interface can propagate over several microns. From the dispersion relation, it is seen that the propagation constant does not go to infinity as the SPP frequency is reached, but folds back and eventually crosses the light line, as is true for SPPs propagating at single interfaces. Large propagation constants can be achieved for excitation well below the SPP frequency provided the width of the dielectric layer is in the order of $\lambda/2$. Adjusting the thickness of the dielectric region provides access to larger propagation length and smaller field penetration into the metallic layers.

1.2 THz TIME DOMAIN SPECTROSCOPY

Figure 1.6 shows the THz time domain spectroscopy (THz-TDS) setup used for our experiments. It consists of a femtosecond (fs) Ti: Sapphire (10 fs pulse-width) laser with 800nm wavelength and repetition frequency of 76 MHz. The optical pulses are focused onto the inner edge of the input terminal of a coplanar strip line on a biased semi-insulating LT: GaAs wafer. Each pulse creates an electron-hole pair and the subsequent acceleration of these carriers by the bias field, generates a near single-cycle linearly polarized electromagnetic pulse of THz radiation. In the standard THz TDS setup, the sample under investigation is placed at the beam waist between the two off-axis parabolic mirrors, which are in the confocal configuration. The transmitted THz is collected by another pair of parabolic mirrors and detected by a ZnTe <110> based electro-optic detection setup.

The transmitting antenna is at the focus of a hyper hemispherical lens, made of high resistance silicon, which collimates the far field pattern into a Gaussian beam with a $1/e$ beam width of 5 mm. The beam waist forms in the focal plane of the parabolic mirror, which focuses the beam to a second beam with diameter (200 μ m) proportional to the wavelength. The combination of the parabolic mirror, silicon lens and antenna chip constitutes the THz transmitter, which generates a highly directional, freely propagating beam of picosecond THz pulses.

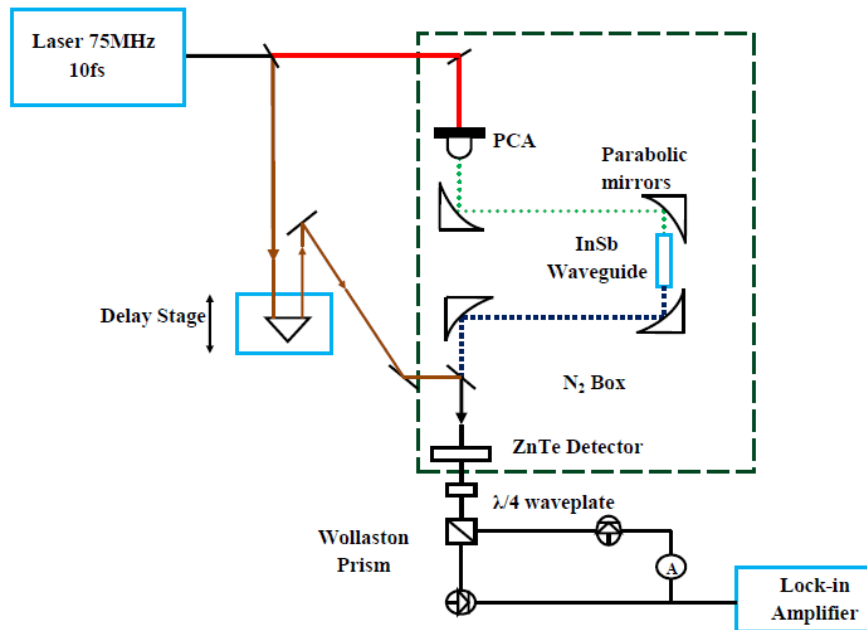


Figure 1.6: Standard THz time domain spectroscopy (THz TDS)

The dotted line in figure 1.6 is a box, partially sealed and connected to dry nitrogen tank creating a low humidity environment inside. This is required as even a small trace of water in the THz beam path will absorb a large amount of the radiation.

The ultra short pulse in the detection path is incident upon a retro-reflector on an electro-mechanical delay line called the delay stage. This delay stage enables us to delay the laser pulse accurately relative to the THz pulse signal from the sample.

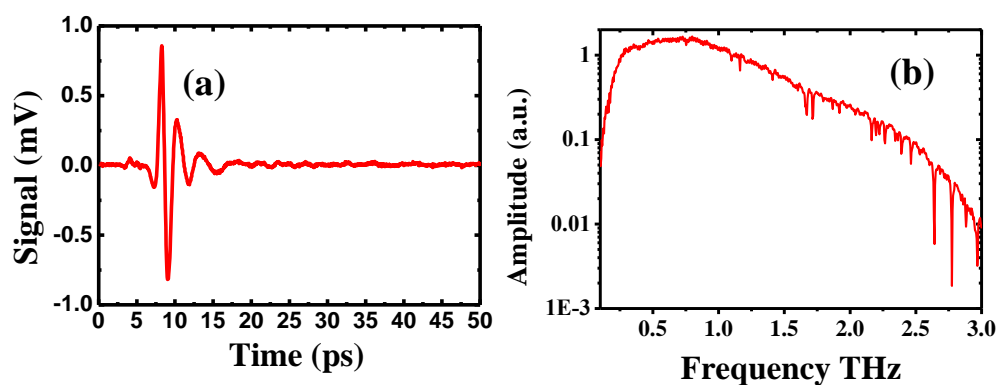


Figure 1.7: Typical traces of the THz Time domain spectroscopy. (a) Raw data in the time domain (b) Corresponding numerical Fourier transform of the time domain signal.

At the detection end, the THz pulse and the probe pulse propagate in the detection crystal, a ZnTe crystal of thickness 0.5 mm. The beam then passes through a quarter-wave plate and Wollaston prism that splits the beam into two plane polarized light beams. These two beams are focussed onto the two photo-diodes of the differential detector. The difference in the signal is sent to the lock-in amplifier. This measured difference in the intensity of the two beams is directly related to the terahertz electric field strength. Thus the terahertz field can be plotted against time. An example of this is shown in figure 1.7a. The Fourier Transform of the temporal THz pulse is computed to obtain the frequency spectrum of the THz electric field (Figure 1.7b).

1.3 LITERATURE REVIEW

Earliest work related to plasmonics dates back about 100 years when Sommerfeld (1899) and later Zenneck (1907) presented theoretical analysis of surface waves on metal surfaces. Equally important was the seminal work of Paul Drude (1900) on conductivity of metals, which in turn can be related to the refractive index of metals. The next important development was the classic work of Ritchie (Ritchie 1957) in which he demonstrated the excitation of surface plasmon waves in experiments on electron diffraction by thin metal foils. A little later in 1968, Kretschmann and Raether showed that surface plasmon waves can be excited optically on metal surface by employing the prism-coupling technique (Sambles et al. 1991). Thus the phenomenon of Surface Plasmon Polariton (SPP) was established. These developments led to research on several devices, all working at optical wavelengths. Much of the past works have been well described in the monograph on “Surface Plasmons” by Heinz Raether (1988). Further, towards the end of 20th century, interest in plasmonic devices operating at Terahertz frequencies picked up. The last 15 years have seen a rapid growth of research in this new domain of Plasmonics. In what follows, we present a brief summary of the literature on plasmonic devices over the past two decades.

1.3.1 Surface Plasmons

Waveguides are used for a controlled transport of electromagnetic radiation with minimum loss and dispersion (Keiser 1991). Thus waveguides, especially thin film stripe or channel types, are an essential part of any signal processing or imaging or sensing

system/chip. Initial studies focused on thin film waveguides having either Insulator-Metal-Insulator (IMI) or Metal-Insulator-Metal (M-I-M) configuration designed for optical wavelengths (Burton and Cassidy 1990, Prade et al. 1991, Berini et al. 1996, Tournois and Laude 1997, Berini et al. 2000). Experimental confirmation of the existence of surface plasmon waves was reported very soon (Marti et al. 1993, Webber et al. 2001) and the young field of plasmonics rapidly expanded in new directions in the late 1990s and early 2000s.

At that time it was demonstrated that plasmon propagation in,

- Metallic nanowires can guide light well below the seemingly unsurpassable diffraction limit (Takahara et al. 1997).
- Metal film with nanoscale holes show extraordinarily high optical transmission (Ebbesen 1998).
- Simple thin film of metal can serve as an optical lens (Pendry 2000).

Diffraction of waves limits the size of the aperture for light transmission. However, metallic thin films, with an array of apertures, yielded unusually high light transmission at wavelengths as large as ten times the diameter of the aperture (Pendry et al. 2001, Ebbesen et al. 2002). This phenomenon was related to excitation of surface plasmon (SP) waves at the metal interfaces, leading to extraordinarily high light transmission.

Propagation of surface plasmon waves on a flat metal surface gets significantly attenuated owing to absorption in the metal. This attenuation depends on the dielectric properties of the metal at the frequency of the SP waves (Barnes et al. 2003). Studies on thin film stripe of gold on a glass substrate (Lamprecht et al 2001) revealed bound SP mode propagation at the metal dielectric interface. Devices having MIM geometry, made using thin film of Au or Cu or Al metal, show higher confinement of SP mode compared to a device in the IMI geometry (Zia et al. 2004). SP wave propagation in triangular (V) groove on gold films (Bozhevolnyi et al. 2005) and plasmon slot waveguide (Veronis et al. 2007) at telecommunication wavelength (1425 – 1620nm) showed low-loss for a waveguide of width of 600nm and film thickness of 1 μ m; propagation length of 100 μ m was achieved.

Further advances on plasmonic MIM waveguide devices focused on waveguides with stubs (Matsuzaki et al. 2008) and bends (Veronis et al. 2005). Studies on optical transmission of these devices revealed that they function as narrow band optical filters on account of interference occurring between the waves travelling in the forward and reverse

directions. This aspect was explored analytically by modeling the devices as equivalent RLC circuits derived from Transmission Line theory (Pannipitiya et al. 2010).

Investigations on the dispersion relations and wave attenuation in two-dimensional Ag/SiO₂/Ag structures for waveguide thickness ranging from 12 nm to 250 nm (Dionne et al. 2005, Dionne et al. 2006) led to better understanding of MIM type devices (Stefan Maier 2006). Characteristics of forward and the backward propagating guided SP waves was studied taking wave energy losses into account (Bozhevolnyi et al. 2010). MIM waveguide device made using gold film of thickness 60nm, (Yang et al. 2014) was observed to show highly efficient SP wave excitation and propagation. Very recently, plasmonic devices have been made using Graphene (Stefan Maier 2012). Such devices show strong mode confinement, wavelength tunability and long lived collective plasma oscillations (Grigorenko et al. 2012). Graphene plasmonic waveguide, with a monolayer of graphene on dielectric substrates has the potential to provide smaller loss and longer propagation lengths (Vakil et al. 2011, Zhu et al. 2013, Zheng et al. 2015).

Compared to the studies on plasmonic devices at visible light frequencies, fewer works have been reported on devices operating in the terahertz frequency regime (Masayoshi 2007, Isaac et al. 2008, Gallant et al. 2007, Vinconzo et al. 2010). This dissertation focuses on the properties of SP wave propagation in THz waveguide device and its application as chemical sensors.

1.3.2 Terahertz waveguide devices

THz pulses of subpicosecond duration were first generated using optoelectronic methods (Auston et al. 1980) using coplanar waveguide devices. However, pulse distortion due to frequency dependent loss and dispersion (Cooper 1985) was a problem. This was overcome by the use of photoconductive dipole antenna (PCA) for generating and detecting THz pulses, avoiding the use of waveguides (Auston 1984). Subsequently, techniques were developed to improve the coupling efficiency of the generated and detected pulse (Fattering et al. 1988, McGowan et al. 1999). New designs of PCA also emerged with increased power and operation bandwidth. These new sources were used for free space propagation with very low loss.

In the early 1990's biomedical applications of THz radiation were limited by large diffraction limited focal spot size, requiring the use of large sized bio-samples. This

problem may be overcome by using waveguide devices. However, guided wave devices suffer from excessive power loss and pulse distortion. Towards the end of 1990's, ways to overcome these hurdles were proposed by Daniel Grischkowsky and others (McGowan et al. 1999, Grischkowsky 2000). The new waveguide devices were robust and were simple to integrate into the already available THz systems. More importantly, they allow stronger interaction between the THz radiations with the sample loaded into the waveguide.

THz waveguides were fabricated by sawing a 270 μ m wide slit through a 40 mm wide and 300 μ m thick silicon slabs with subsequent metallization of all faces. Low-loss propagation with negligible group velocity dispersion was observed in the 0.1–1 THz frequency range (Wächter et al. 2007). Sub-wavelength array of rectangular slots in semiconductors (Silicon and Indium Antimonide) exhibited stronger electric field at the edges, compared to metal slots, on propagation of THz radiation through periodic structures (Gelmont et al. 2008). It was suggested that such field enhancement is due to excitation of surface plasmons. This phenomenon may be exploited in novel bio-sensors. The potential for sensor applications has driven intensive investigations on different waveguide structures using a variety of materials, both metals and semiconductors. Some of the significant contributions on the characteristics of THz plasmonic devices are:

- THz SP localization within a nanoporous silicon slab (Lo et al. 2010).
- Periodic rectangular apertures on metal foil as a complex planar plasmonic THz waveguide device (Zhu et al. 2011).
- Subwavelength confinement of THz SP in tapered parallel plate waveguide (PPWG). (Zhan et al. 2011).
- Micromachining rectangular stubs on PPWG as resonant cavity to observe electromagnetically induced transparency (EIT) (Mendis et al. 2009, Chen et al. 2013, Kimberly et al. 2014, Steven 2014).

In any plasmonic device, excitation of surface plasmon waves is a prime requirement. While metals, like gold and silver, are suitable for optical radiations, semiconductors are appropriate for devices designed to work at THz frequencies since they have a much lower permittivity than metals at THz frequencies. Further, their much lower free carrier concentration leads to plasma waves in the THz regime. For waveguide device made of semiconductors, their permittivity allows for a strong coupling of the THz field to free charges at the semiconductor-dielectric interface resulting in a propagating surface wave. Further, the carrier concentration in semiconductors may be modulated thermally or

optically, besides appropriate doping, to match a specific THz frequency, making them promising candidates for tuneable plasmonic devices in the THz domain.

THz radiation may be used to probe the vibration and rotational modes of biomolecules, like proteins, DNA, RNA, leading to a variety of promising bio and chemical sensors. Such studies were carried out by the technique of THz Time Domain Spectroscopy (TDS) since early 2000. Initially the samples were taken in cuvettes and, hence, required large quantities of the sample. Later several groups worked on THz Plasmonic devices and demonstrated detection with high sensitivity. Some of the significant contributions on such plasmonic sensors are listed below:

- ❖ PPWG devices for high resolution THz spectroscopy to study a specific vibration mode for several protein molecules (Laman et al. 2008)
- ❖ THz antenna (Berrier et al. 2012) was used to detect bacterial layers with high sensitivity. These THz sensors can sense ultra-thin (a few nanometer thick) molecular layers (John et al. 2008) and a few femto-moles of DNA molecules.
- ❖ THz dielectric pipe waveguide was used for detecting vapours of hydrochloric acid, acetone, ammonia and water with a minimum detectable molecular density as low as 1.6 nano-mole/mm³ (You et al. 2012).
- ❖ A THz metamaterial device, consisting of symmetric split ring resonators, was exploited as ultrasensitive refractive index sensor, possessing a sensitivity of 36.7 GHz/RIU and 23.9 GHz/RIU when Fano and Quadrupole resonances, respectively, were excited (Singh et al. 2014).

1.4. SCOPE AND OBJECTIVES OF THE THESIS WORK

Terahertz science is acquiring multi-disciplinary dimensions. It has drawn ideas from photonics, electronics, material science and nanotechnology and has applications in signal processing, spectroscopic analysis of materials, detection of explosive and hazardous materials and sensors. Plasmonic sensors at THz frequencies are especially suited for sensing bio-molecules.

This thesis focuses on developing a novel THz plasmonics sensor consisting of a waveguide, with stubs along the waveguide. Such devices exploit the phenomenon of surface plasmon waves and function as resonant devices. The resonant characteristics of

the device lead to strong localization of electric fields in the stubs and this facilitates a strong interaction of the THz wave with any material present in the stub. Waveguide devices were fabricated using intrinsic Indium Antimonide (InSb) and their propagation characteristics at THz frequency were experimentally investigated. The sensing property of the device was also studied. The main research objectives of the Thesis were:

1. To model the dielectric properties of Indium Antimonide at THz frequencies.
2. To study the transmission characteristics of InSb plasmonic devices using simulation tools such as COMSOL Multiphysics and Ansoft HFSS.
3. To model the plasmonic device as an equivalent RLC circuit.
4. To fabricate the designed InSb plasmonic device by laser micromachining.
5. To investigate the transmission characteristics of the waveguide without stub (straight waveguide) and waveguide with two stubs using THz TDS technique.
6. To investigate the sensing capability of the device by loading the protein Bovine Serum Albumin (BSA) and polystyrene dissolved in toluene into one of the stubs of the device and measuring the transmission coefficient using THz TDS technique.

The work presented in the thesis is divided into six chapters. A brief summary of the contents of each chapter is given below.

Chapter 1 contains a general introduction to Plasmonics, theoretical aspects of surface plasmon propagation at metal – dielectric and metal- dielectric-metal interfaces. Next, the details of THz TDS technique are discussed. Literature survey of the research work on THz waveguide devices and their applications as chemical and biosensor are presented. The scope and objectives of the present work are mentioned at the end of this chapter.

Chapter 2 presents the relevance of semiconductors for THz devices, modelling of the frequency dependent dielectric permittivity of InSb using Drude free electron model along with simulation and numerical investigation of THz InSb plasmonic waveguide using effective index method (EIM). Effective index approach is applied for modelling surface plasmon polaritons (SPPs) propagation in InSb planar waveguide. The effective index of the propagating mode along with the corresponding propagation lengths are calculated for different configurations at THz wavelengths while varying the trench

depth. The confinement of SPPs in the trench along with the variations in the propagation length for different trench dimensions is discussed.

Chapter 3 describes the simulation studies using COMSOL Multiphysics and Ansoft HFSS on THz InSb waveguide with stubs along the waveguide acting as resonant cavity leading to a narrow band filter. The transmission characteristics and the resonance features of the waveguide with single and two stubs have been discussed for various device dimensions like waveguide width and stub length. An attempt has been made to establish an analogy between InSb waveguide and microwave transmission line by modelling the device as an equivalent RLC circuit. The transmission spectra of the simulated and analytically calculated InSb waveguide with stub are compared and discussed.

Chapter 4 reports the experimental investigation of THz InSb waveguide device including fabrication and characterization using THz TDS. The detailed steps involved in the preparation of InSb pellets, the creation of trench by laser ablation to form waveguide and stubs on the upper face of the pellet are presented in the first section. THz TDS on the fabricated InSb waveguide devices showing the dependence of resonance frequency on waveguide with stub are discussed. Comparison of the simulated and experimental transmission spectra of the waveguide with stub is made and the plasmon propagation, together with narrow band filtering characteristics of the waveguide, is also discussed. Above the cut off frequency the device shows transmission maxima and minima as a function of frequency. This can be attributed to the interference between the forward propagating wave and the wave reflected from the stub.

Chapter 5 focuses on exploiting the resonance characteristics of the THz InSb waveguide device as a novel sensor. A well known protein molecule, Bovine serum albumin (BSA) and polymer sample, polystyrene dissolved in toluene, are used for evaluating the sensing capability of the waveguide. Loading one of the stubs in the device with one of the sample materials, changes the refractive index of the medium inside the stub. The change in the transmission and absorption coefficient of the device by varying the concentration of the medium is studied and presented. Substantial improvement in the sensitivity of the device for only a few micro litre quantity of the sample is observed. The potential application of InSb waveguide as a promising sensor is discussed.

Chapter 6 summarizes the main results and conclusions of this research work. Suggestions for future research on this topic are mentioned. The chapter ends with references, a list of publications and the author's bio-data.

CHAPTER 2

MODELLING OF InSb PLASMONIC THz WAVEGUIDE

Abstract

In this chapter we present the results of modelling and simulation of the propagation characteristics of electromagnetic waves, at THz frequencies, in a channel waveguide made using InSb. We focus on SPP propagation along the semiconductor-insulator (SI) interface. The Effective Index method has been employed to study the SP propagation in the channel waveguide of sub-wavelength width. We have investigated the strength of the wave electric field close to the interface and also the propagation losses at THz frequencies.

2.1. INTRODUCTION

THz plasmonic devices exploit the coupling of THz electromagnetic waves with the collective oscillation of the free electrons in the medium. This coupling of the wave to the surface is maximum for frequencies close to the plasma frequency of the metal or semiconductor. The plasma frequency of metals lies, typically, in the visible or ultraviolet part of the electromagnetic spectrum. At THz frequencies the EM wave is no longer a surface wave for metals as the electromagnetic fields get highly delocalized.

Semiconductors have a much lower plasma frequency than metals, typically in the terahertz frequency range, allowing strong localization of THz SPPs to the semiconductor-dielectric interface. Another crucial difference between metals and semiconductors is that semiconductors are much more versatile materials since their plasma frequency may be tuned by appropriate doping. Switching of the SPP-assisted resonant THz transmission through hole arrays has been demonstrated using electrical (Chen et al. 2008), optical (Hendry et al. 2008) and thermal (Rivas et al. 2004) techniques. Also efficient real-time control and manipulation of THz SPPs using active metamaterial resonant semiconductor devices enables improved modulation of THz

transmission over existing devices (Chen et al. 2006). Consequently semiconductors are promising candidates for active Plasmonic devices at THz frequencies.

2.2 IMPORTANCE OF InSb IN THE THz FREQUENCY REGIME

Among the III-V binary semiconductors, Indium Antimonide (InSb) has attracted considerable attention over the last several years. Many of its interesting properties are directly associated with its very low effective electron mass and high electron mobility. It has the smallest band gap among other III-V binaries, measuring 0.17eV at 300K that corresponds to IR wavelength and the material is therefore useful as an infrared detector and filter (Koichiro et al. 2013).

In order to fully describe the properties of InSb, relevant to plasmonic devices, the expression for frequency dependent permittivity is required for calculating the attenuation and propagation of SPPs. Time resolved studies of carrier dynamics (electrons and holes) in semiconductors (Exter et al. 1990) have shown that the permittivity of semiconductors at THz frequencies is well described by the Drude model for free electrons.

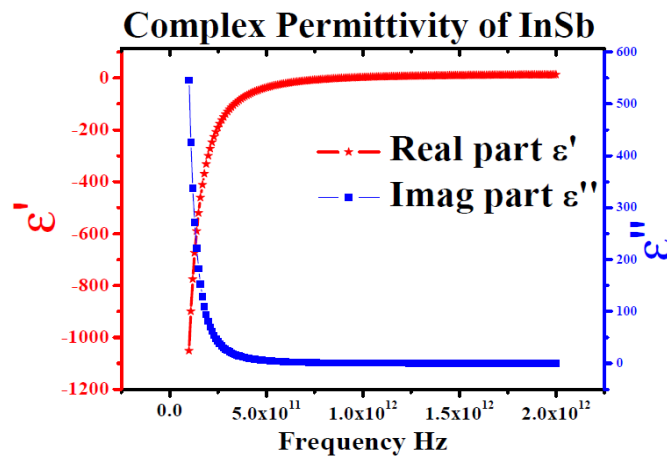


Figure 2.1: Real and Imaginary part of the complex permittivity of InSb calculated using Drude free electron model.

The expression for the dielectric permittivity is given by

$$\varepsilon(\omega) = \varepsilon_{\infty} - \frac{\omega_p^2}{\omega^2 + i\gamma\omega} \quad (2.1)$$

where, the high frequency permittivity $\epsilon_\infty = 15.75$, $\gamma \sim 1.25$ THz is the carrier collision frequency for InSb and the plasma frequency is given by $\omega_p^2 = \frac{Ne^2}{\epsilon_0 m^*}$ which depends on the electron number density N and its effective mass m^* ; for InSb $m^* = 0.014 m_e$, where m_e is the free electron mass.

The carrier density depends significantly on temperature, doping level and on absorption of visible light photons. The intrinsic carrier density N of InSb (Jin et al. 2013) is given by $N = 5.76 \times 10^{14} T^{1.5} \exp(-0.129/k_B T) \text{ cm}^{-3}$. At 300K the $\epsilon(\omega)$ of InSb at 0.3THz is $-91.54 + 15.67i$ which is similar to that of metals at optical frequencies.

From the expression of the plasma frequency, it follows that the permittivity depends on the carrier concentration and carrier mobility. The plasma frequency for InSb is in the THz range. Therefore the value of permittivity of InSb at THz frequencies is close to that of metals in the visible and near infrared frequencies, i.e. the permittivity has a real negative part with a small absolute value and a small imaginary component related to energy absorption. In contrast, the permittivity of gold at THz frequencies has a very large negative real value and a large imaginary component. These values, several orders of magnitude larger than those of InSb are due to the higher plasma frequency of gold compared to InSb. The difference in plasma frequency between InSb and gold is mainly determined by the much higher free carrier density of metal. Hence, just as metal surfaces support SPPs at visible frequencies it is expected that SPPs should also propagate on the surface of InSb at THz frequencies.

2.3. SURFACE PLASMON MODES IN InSb WAVEGUIDE

Propagation properties of THz InSb waveguide structures were simulated and analyzed using COMSOL Multiphysics and Ansoft HFSS softwares. The frequency dependent permittivity of InSb at THz frequencies was calculated using Drude model. The waveguides were modelled as a channel waveguide surrounded by air with spatial grid size chosen to ensure convergence of the numerical calculations. Perfectly matched layer

absorbing boundary conditions were applied at all the boundaries. TM polarized THz wave was incident on the input port. SPP propagation along the waveguide and the dependence of the transmission characteristics on the waveguide dimensions were analyzed.

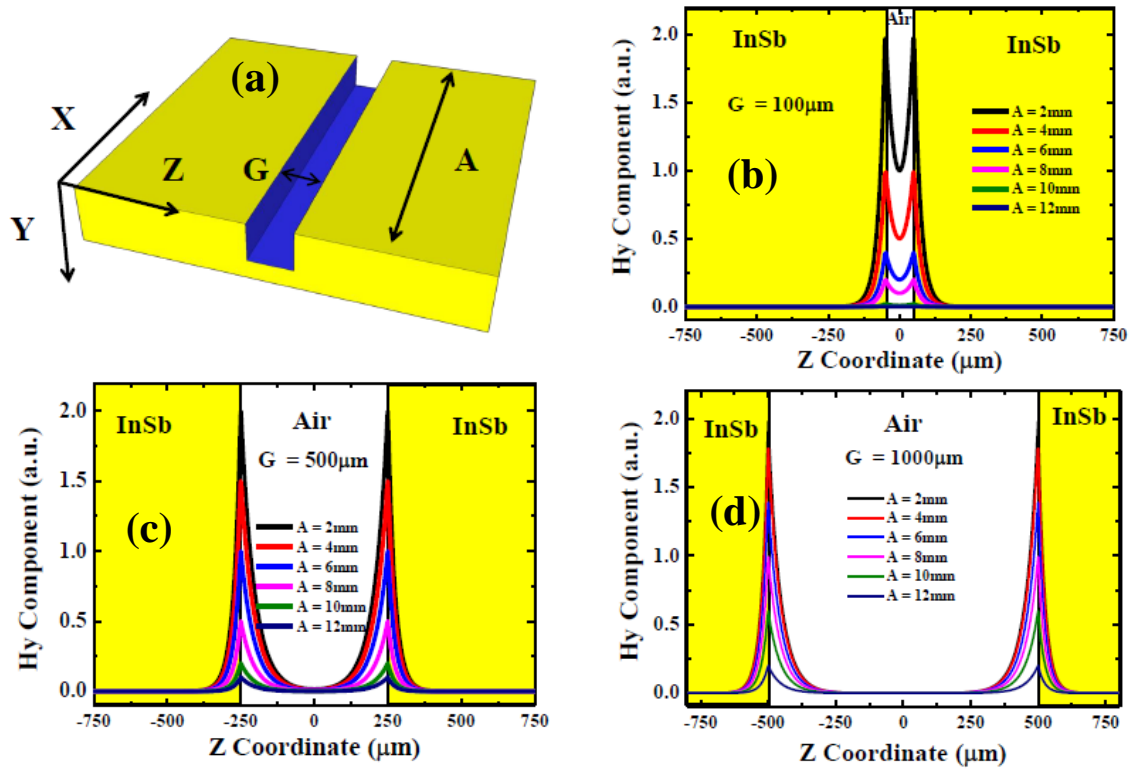


Figure 2.2 (a) Schematic of InSb channel waveguide of width G and length A . Transverse H_y component of the TM SPP propagating along the SIS interface for (b) $G = 100 \mu\text{m}$, (c) $G = 500 \mu\text{m}$, (d) $G = 1000 \mu\text{m}$ at different length A of the InSb channel waveguide.

Figure.2.2 shows that the guided mode pattern depends on the width of the waveguide. Theoretical analysis indicates that the cut-off frequency of the waveguide with rectangular cross section depends solely on the depth (D) of the waveguide (Zhu et al. 2011); cut-off frequency $f_c = c/2D$. The propagation characteristics of InSb channel waveguide of depth (D) = $1800 \mu\text{m}$ were obtained by simulation for varying waveguide width G . Figure 2.2b shows the H_y component of the SPP mode for $G = 100 \mu\text{m}$, $500 \mu\text{m}$ and $1000 \mu\text{m}$ with the decay length of $\sim 50 \mu\text{m}$, $\sim 120 \mu\text{m}$, $\sim 150 \mu\text{m}$ respectively. The mode field associated with the propagating mode has a large transverse (H_y) component. As the width of the waveguide decreases, the intensity of the H_y component leaking into

the semiconductor waveguide increases and the propagation length of the mode along the waveguide decreases. Such waveguide devices exhibit strong attenuation of the wave.

Semiconductors are generally lossy and, hence, the SP modes of a semiconductor-dielectric structure can propagate over several microns. However, in our devices made of InSb a relatively small portion of the wave energy is carried in the dissipative InSb layer and hence the mode can propagate over distances of the order of a few millimetres. This aspect is suitable for THz integrated circuits and interconnects and has inspired a new class of plasmon channel waveguides in the THz domain. (Jin et al. 2013)

2.4. EFFECTIVE INDEX METHOD ANALYSIS OF THz InSb WAVEGUIDE

Analysis of 2-dimensional rectangular waveguides often requires numerical computation. Based on perturbation techniques, a simple numerical method called Effective Index Method (EIM) was developed in early 1970s (Knox and Toullos 1974, Hocker et al. 1977).

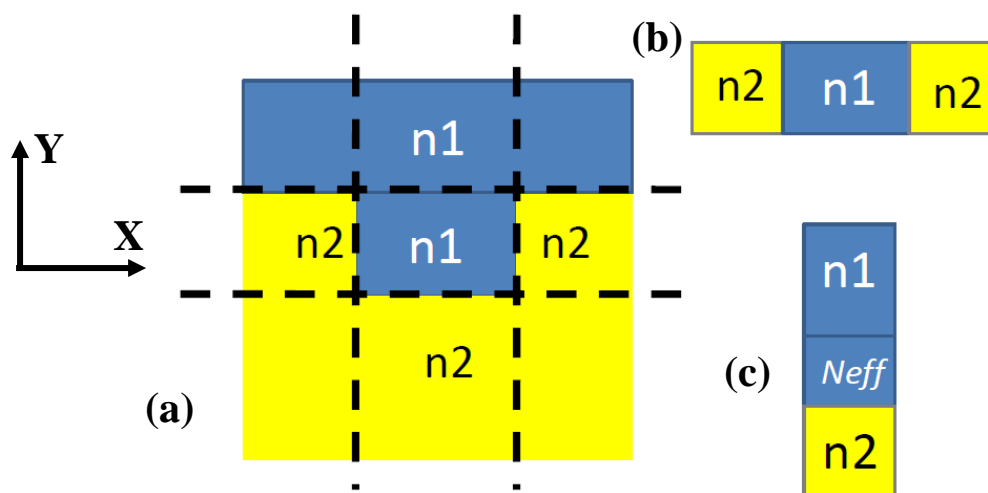


Figure 2.3 (a) Schematic of InSb channel waveguide for effective index method analysis. (b) Planar slab waveguide I (c) waveguide II configuration in determining the effective refractive index of the InSb channel waveguide.

This method has been widely used for analysing waveguide devices (Bozhevolnyi et al. 2005). In this method a 2-dimensional rectangular waveguide is treated as a combination

of two slab waveguides (labelled here as waveguide I and II) oriented perpendicular to each other. Essentially the solutions for a 2-dimensional waveguide problem are obtained in terms of solutions for two 1-dimensional problems.

We consider a channel waveguide as shown in figure 2.3. To apply the effective index method, waveguide I (Figure.2.3b) is treated as a slab waveguide extending in the y-z plane. Modal analysis of this slab waveguide yields the value of propagation constant β of the mode of our interest and using this, the effective index, n_{eff} , is calculated using

$$n_{\text{eff}} = \frac{\beta}{k_0} \quad (2.2)$$

where k_0 is the wave number in vacuum. This effective index is now assumed to be the refractive index for the core region of waveguide-II, which is also a slab waveguide extending in the x-z plane (Figure 2.3 (c)). It may be noted that with this prescription, waveguide-II becomes an asymmetric waveguide. Modal analysis of waveguide-II yields the propagation constant (β) for the desired mode, which should be a TM-mode in order to represent SPP mode for the channel waveguide. It is easy to see that only a TE-mode of waveguide-I leads to the TM-mode for waveguide-II.

We have carried out the modal analysis for TE-mode for waveguide-I using the following characteristic equation to determine β for the symmetric mode,

$$\tanh(k_d G) = \frac{2k_d \gamma_s}{k_d^2 - \gamma_s^2} \quad (2.3)$$

where $\gamma_s^2 = \beta^2 - k_0^2 \epsilon_s$ and $k_d^2 = k_0^2 \epsilon_d - \beta^2$, k_0 is the free space wave number of the electromagnetic wave. The solution of the above equation yields β values for the guided mode and using this value n_{eff} can be calculated from Eq.2.2.

Waveguide-II as shown in Figure.2.3(c) is an asymmetric slab waveguide. For waveguide-II the mode being considered assumes TM-mode polarisation due to its different orientation with respect to waveguide-I. Hence, we have computed the propagation constant β for TM-mode for waveguide-II using the following characteristic equation appropriate for TM modes in asymmetric waveguide

$$\tanh(k_f G) = \frac{k_f \left[\frac{N_{eff}^2}{n_2^2} \gamma_s + \frac{N_{eff}^2}{n_1^2} \gamma_c \right]}{k_f^2 - \frac{N_{eff}^4}{n_1^2 n_2^2} \gamma_c \gamma_s} \quad (2.4)$$

where $\gamma_s^2 = \beta^2 - k_0^2 \epsilon_s$, $\gamma_c^2 = \beta^2 - k_0^2 \epsilon_d$, $k_f^2 = k_0^2 \epsilon_f - \beta^2$, $\epsilon_f = N_{eff}^2$, $\epsilon_d = n_1^2$, $\epsilon_s = n_2^2$, k_0 is the free space wave number of the electromagnetic wave. In the calculations we have set $\epsilon_d = 1.0$ for the dielectric layer and for the dielectric permittivity of InSb at 0.3 THz we have set $\epsilon_s = (91.54 + 15.67i)$. The propagation constant β , thus determined, is taken as the actual value for the SPP mode of the channel waveguide. We have computed β for varying waveguide width (G) and also waveguide depth (D). The results of the computations are displayed as graphs shown in Fig. 2.4 and 2.5.

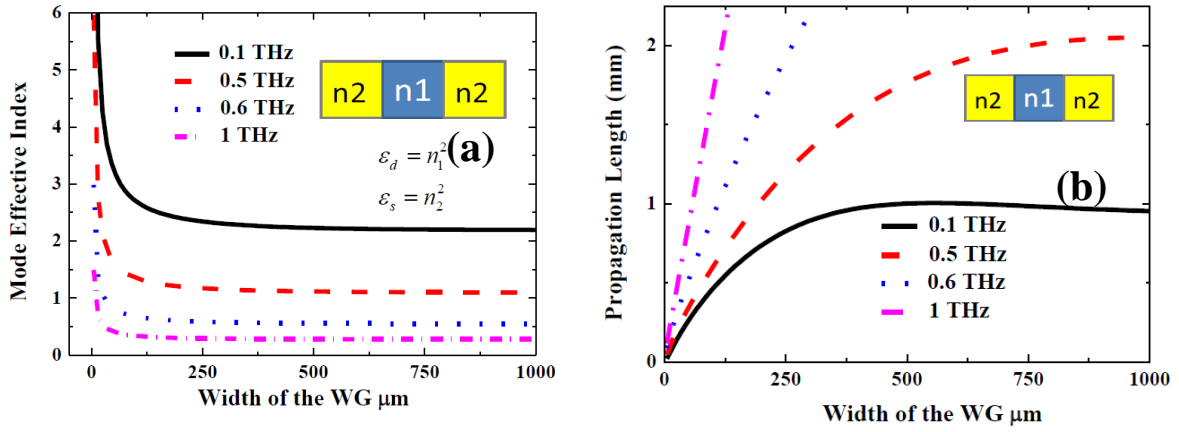


Figure 2.4 The SPP mode (a) Effective index and its (b) Propagation length as a function of the width G of the InSb waveguide at THz frequencies.

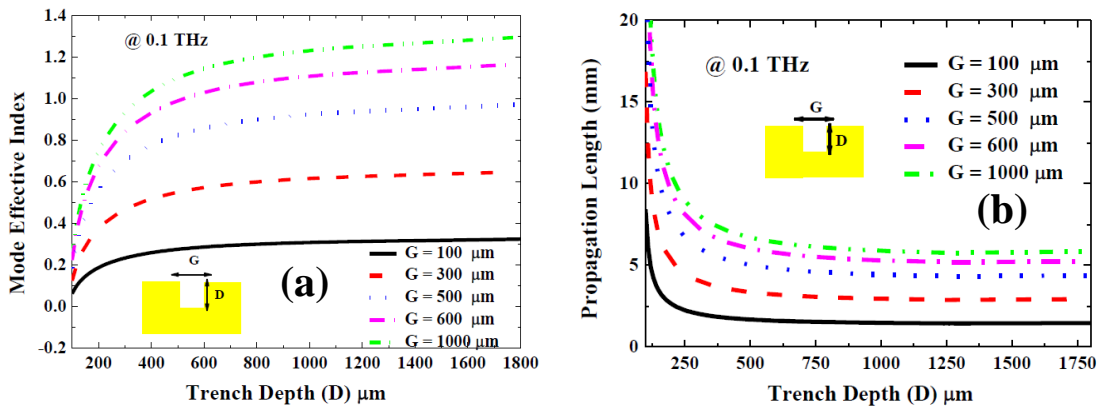


Figure 2.5 (a) Mode effective index and (b) propagation length as a function of the depth (D) of the InSb waveguide at 0.1 THz. Parameter ranges correspond to the single-mode waveguiding regime. The inserts show the cross sectional geometry of the InSb waveguide.

Investigations on the waveguiding properties, i.e., mode effective index, propagation length, have been performed for wavelengths in the THz range. In regard to the mode confinement it is advantageous to keep the depth of the waveguide (D) as large as possible, as it decides the cut-off frequency of the waveguide. The choice of waveguide width (G), however, is slightly more complicated and is subject to a trade-off between mode confinement and propagation length. Although the mode effective index increases monotonously with increase in waveguide width (G), the mode width has a distinct minimum. This can be envisaged as a point where the field is squeezed into the waveguide sub-region and when the width is decreased until a certain point, where the field no longer can be confined to the depth. It then starts to spread out in the surrounding semiconductor interfaces, where the decay length is larger, thereby increasing the mode width. These considerations have led to a determination of the optimum waveguide parameters $G \sim 750 \mu\text{m}$ and $D \sim 1500 \mu\text{m}$, which ensures mode propagation with sub-wavelength lateral confinement. A wavelength analysis of the guiding properties of the InSb waveguide using EIM has been verified by measurements performed on fabricated samples with dimensions close to the optimum and is described in the next chapter.

2.5. CONCLUSIONS

In summary, InSb THz waveguide supports SPP propagation along the semiconductor insulator interfaces and the geometrical parameters were optimized to obtain longer propagation length. The propagation characteristics of InSb channel waveguide were obtained by simulation for varying waveguide width (G). H_y component of the SPP mode for the InSb waveguide of width $G = 100\mu\text{m}$, $500\mu\text{m}$ and $1000\mu\text{m}$ had a decay length of $\sim 50 \mu\text{m}$, $\sim 120 \mu\text{m}$, $\sim 150 \mu\text{m}$ respectively. The mode field associated with the propagating mode has a large transverse (H_y) component. As the width of the waveguide decreases, the intensity of the H_y component leaking into the semiconductor waveguide increases and the propagation length of the mode along the waveguide decreases. Effective Index Method has been applied for modelling the SPP propagation in the rectangular channel waveguide. Investigation on the waveguiding properties, i.e., mode effective index, propagation length, has been performed for wavelengths in the THz range. The method has led to a determination of the optimum waveguide parameters $G \sim 750 \mu\text{m}$ and $D \sim$

1500 μm , which ensures mode propagation with sub-wavelength lateral confinement. A wavelength analysis of the guiding properties on the InSb waveguide using EIM has been verified by measurements performed on fabricated samples with dimensions close to the optimum and is described in the next chapter.

CHAPTER 3

TRANSMISSION CHARACTERISTICS OF THE InSb PLASMONIC DEVICE

Abstract

This chapter presents simulation studies on SPP propagation and the filtering properties of InSb waveguide device with (a) single and (b) two pair of stubs which functions as a cavity resonator at THz frequencies. With the excitation of localized SPs, the study focuses on the transmission and filtering properties of the waveguide for different stub length and stub width. These waveguide devices with stubs resonate at particular frequencies called the resonant frequencies and transmitting all other frequencies. Simulation studies indicate large electric field enhancement in the stubs at resonance, which is also supported by analytical calculations using the methods of microwave transmission line network theory.

3.1. INTRODUCTION

The availability of THz sources and detectors has led to rapid progress in the development of plasmonic waveguide components such as polarisers, filters and collimators (Masayoshi 2007). In this chapter, we investigate the transmission characteristics of InSb waveguide device having single and two pair of stubs at THz frequencies using COMSOL MULTIPHYSICS and Ansoft HFSS software packages. The filtering characteristics of the device are studied by simulation. Further, a Transmission Line model is adopted for the device and its transmission characteristics are evaluated and compared with the simulation results. The investigations have been carried out by varying device parameters such as waveguide width, stub length and stub width for devices with a single stub and two stubs. These studies have been carried out to investigate the resonance features of the devices and the localization of the wave electric fields along the device, with particular focus on the stubs. The

strength of the electric fields in the stubs would reveal the potential of the device as a sensor of different materials.

3.2 InSb THz PLASMONIC WAVEGUIDE WITH STUBS

3.2.1 Device Configuration

The schematic of the THz InSb Plasmonic waveguide device investigated in this thesis is shown in figure 3.1. It consists of a planar semiconductor-insulator-semiconductor (SIS) structure (discussed in chapter 2) with stubs along the waveguide to form a resonant structure. The waveguide section and the stubs are made by creating a trench in an InSb pellet. COMSOL MULTIPHYSICS and Ansoft HFSS, finite element method based simulation tools, were employed to theoretically analyze its transmission characteristics.

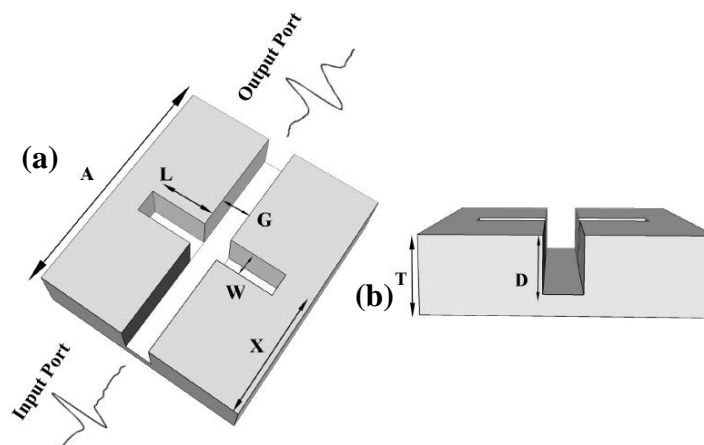


Figure 3.1. Schematic of the InSb waveguide device with two stubs. Typical device dimensions: (a) Stub length $L = 1000\mu\text{m}$, stub width $W = 750\mu\text{m}$, width of the waveguide $G = 750\mu\text{m}$, position of the stub $x = 6\text{mm}$, and length of the waveguide $A = 12\text{mm}$ (b) Depth of the waveguide $D = 1.5\text{mm}$, thickness of the pellet $T = 2\text{mm}$. The parameters G and W are kept equal.

Microwave Resonators are, typically, rectangular cavities with walls made using high conductivity metals. Such structures support standing electromagnetic wave patterns inside the cavity and are characterised by high Quality Factor. They are capable of storing large quantities of electromagnetic energy. Our plasmonic devices also possess the capability to store energy due to the inclusion of the stubs. Since any THz

source has a rather limited output spectrum, these devices are evaluated within this spectrum as a band-pass filter. The resonant frequency for the device can be tuned by varying the device dimensions.

3.2.2 Transmission Characteristics

The THz wave was launched at the input port of the waveguide (Figure. 3.1(a)), exciting the SPP's at the semiconductor-air interfaces in the waveguide channel. The SPP's propagate along the walls of the waveguide and the stubs. The amplitude of the signal exiting the output port was measured. The wave propagates through the device showing frequency dependant transmission minimum and maximum at the output port. Figure 3.2 shows the variation in transmission coefficient as a function of frequency for different values of stub length L , width of the waveguide G .

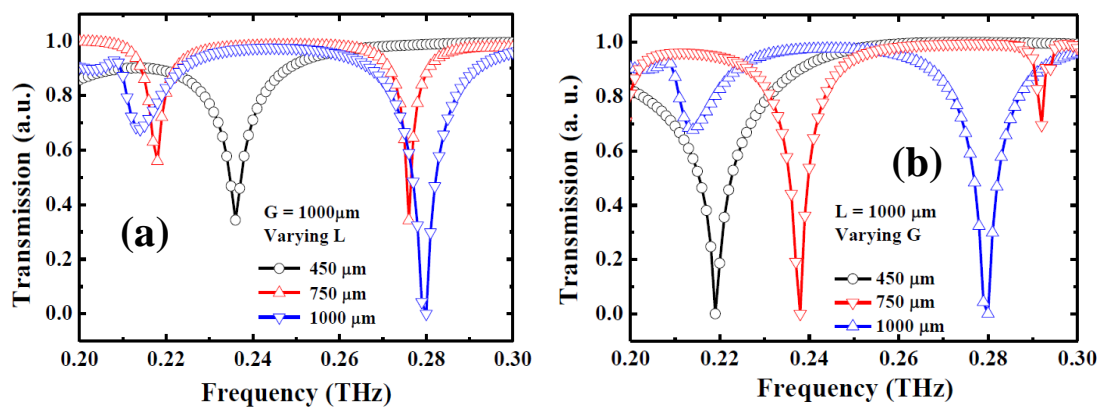


Figure 3.2 Transmission characteristics of InSb THz Plasmonic waveguide device with stubs functioning as a cavity resonator. (a) Varying stub length (L) with $G = 1000\mu\text{m}$ (b) Varying the width of the waveguide ($G = W$) with $L = 1000\mu\text{m}$.

The graphs show sharp dips in the transmission at certain frequencies, known as resonance frequencies, and high transmission over broad frequency ranges. It is seen that, in the frequency range of our interest, for device parameters $L = 450\mu\text{m}$ and $G = 1000\mu\text{m}$, transmission minimum occurs at only one frequency. When L or G was increased, the transmission minima occurred at two or more frequencies. As shown in figure 3.2(a) for $G = 1000\mu\text{m}$ and $L = 450\mu\text{m}$, the transmission minimum occurred at 0.236THz and for $L = 750\mu\text{m}$, minima occurred at two frequencies 0.218THz and

0.276THz. These two minima got slightly shifted to 0.213THz and 0.28THz when L was further increased to $1000\mu\text{m}$. As shown in figure 3.2(b) for $L = 1000\mu\text{m}$ and $G = 450\mu\text{m}$, the device showed transmission minimum at 0.219THz. For $G = 750\mu\text{m}$ minima occurred at 0.238THz and 0.292THz and for $G = 1000\mu\text{m}$ the minima shifted to 0.213THz and 0.28THz. Thus, it is clear that by choosing the sizes G or L , the device can be designed to possess a single or multiple resonance frequencies within the frequency range of the THz source used.

Figure 3.3 shows the electric field pattern of the SPP mode propagating in the device along with the corresponding electron density pattern representing the plasma wave inside the semiconductor. Due to partial reflection of the waves at the stub junction stationary waves exist together with travelling waves in the device. At the resonance frequency the stationary wave formation is maximum leading to overall transmission minima for the device.

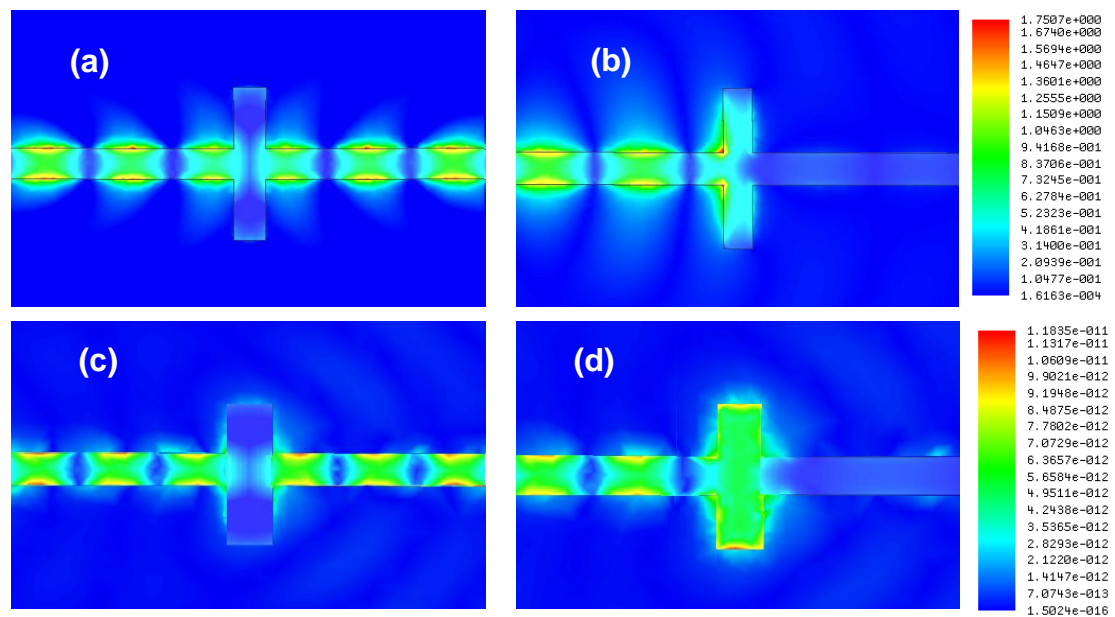


Figure 3.3 Simulated THz electric field and corresponding charge density distribution in the InSb Plasmonic waveguide device with dimensions $G = 750\mu\text{m}$, $L = 1000\mu\text{m}$. (a & c) Indicate maximum transmission at 0.3 THz; (b & d) Indicate minimum transmission at 0.238 THz. (a) and (b) show electric field pattern at 0.3THz and 0.238THz, respectively; (c) and (d) show the charge density profile at 0.3THz and 0.238 THz, respectively.

Figure 3.3(a) shows the electric field profile of the propagating wave at 0.3THz and figure 3.3 (b) shows the pattern at the resonant frequency 0.238 THz for $G = 750\mu\text{m}$ and $L = 1000\mu\text{m}$. Clearly, the resonant dip at 0.238 THz can be correlated to the localization of the electric field of the propagating EM wave in the two stubs leading to strong reflection of the wave back towards the input port. This is also confirmed by the plots of the charge density distribution at 0.3THz and 0.238 THz as shown in figure 3.3 (c) and figure 3.3 (d), respectively. At frequencies away from the resonant frequency, the electromagnetic wave experiences very small impedance mismatch at the waveguide-stub joints and, hence, propagates freely towards the exit of the waveguide indicating high transmission. Further, it is also seen that the magnitude of electric field in the stubs is very small at off-resonant frequencies.

3.3 TRANSMISSION LINE MODEL FOR THE DEVICE

The transmission characteristics of the InSb waveguide with single and more number of stubs can be analysed by using the transmission line theory employed normally at microwave frequencies.

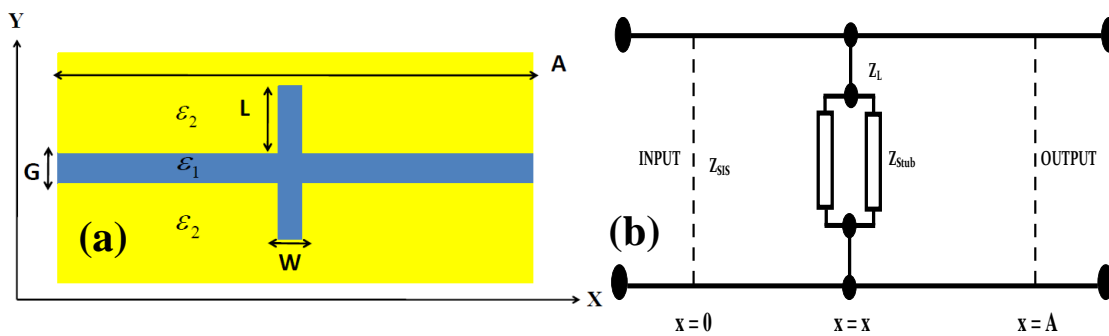


Figure 3.4 (a) Schematics of SIS InSb waveguide device with single stub. (b) Equivalent Transmission line representation with Z_{SIS} the characteristic impedance of the SIS waveguide, Z_{stub} the effective stub impedance, Z_L the load impedance. (Pannipitiya et al. 2010)

The transmission line equivalent circuit for our device is shown in figure 3.4. The infinite transmission line has a characteristics impedance of Z_{SIS} corresponding to the waveguide. The stub along the waveguide is modelled as a finite transmission line

with characteristics impedance Z_C terminated by a load impedance Z_L . The load impedance Z_L is responsible for the reflection and interference of the SPP modes entering and exiting the cavity.

The above mentioned impedances are expressed in terms of device parameters G , W , L , propagation constant (β) and permittivity of the insulator region (ϵ_{air}) and semiconductor (ϵ_{InSb}). The voltage and current wave in a transmission line correspond to the electric and magnetic fields of the SPP mode. Thus the characteristic impedance of the waveguide and the stub has the form (Veronis et al. 2005)

$$Z_{SIS} \approx \frac{E_y G}{H_z} = \frac{\beta G}{\omega \epsilon_0 \epsilon_{Air}} \quad (3.1)$$

$$Z_C \approx \frac{E_y W}{H_z} = \frac{\beta W}{\omega \epsilon_0 \epsilon_{Air}} \quad (3.2)$$

where ϵ_0 is the permittivity of vacuum. It is considered that the energy of the SPP mode is mainly confined in the dielectric region and the transverse electromagnetic field is uniformly distributed along the y axis.

The propagation constant β is calculated from the dispersion relation of SPP modes.

$\tanh\left(\frac{ik_1 h}{2}\right) = \left(\frac{\epsilon_2 k_1}{\epsilon_1 k_2}\right)^{\pm 1}$, where \pm corresponds to the symmetric and antisymmetric

mode $E_x(y) = \pm E_x(-y)$, $k_i = \sqrt{(\epsilon_i k^2 - \beta^2)}$ ($i=1,2$) and ϵ_i corresponds to the relative permittivity of the i th medium.

The load impedance Z_L , accounts for the SPP mode reflection from the ends of the stub. We assume that the SPP undergoes a normal reflection from the stub end and calculate the reflection coefficient using the equation (Pozar 1998)

$$\Gamma = \frac{Z_L - Z_S}{Z_L + Z_S} = \frac{\sqrt{\epsilon_{InSb}} - \sqrt{\epsilon_{Air}}}{\sqrt{\epsilon_{InSb}} + \sqrt{\epsilon_{Air}}} \quad (3.3)$$

which leads to

$$Z_L = \sqrt{\frac{\epsilon_{InSb}}{\epsilon_{Air}}} Z_C \quad (3.4)$$

With the approximation of a perfect electric conductor (PEC) $|\epsilon_{InSb}| \rightarrow \infty$, the amplitude reflectance Γ approached unity and Z_L tends to infinity. Thus the waveguide device with stub is equivalent to an open circuit rather than a short circuit transmission line. The value of Z_{stub} can be obtained from transmission line theory as (Pozar 1998)

$$Z_{Stub} = Z_S \frac{Z_L - iZ_S \tan(\beta L)}{Z_S - iZ_L \tan(\beta L)} \quad (3.5)$$

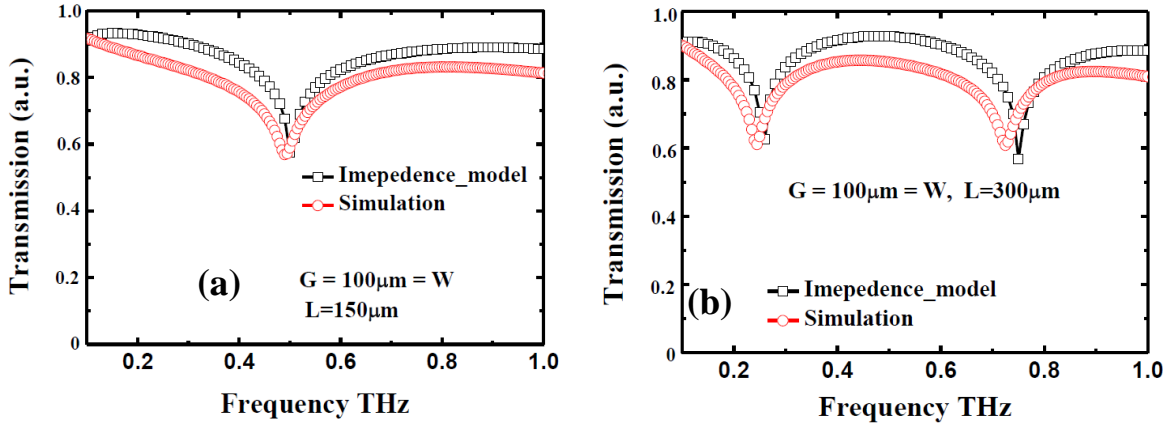


Figure.3.5: Comparison of the transmission line impedance model and the simulated transmission characteristics of InSb waveguide with $G = 100 \mu\text{m}$ (a) $L = 150 \mu\text{m}$ (b) $L = 300 \mu\text{m}$

The transmittance of the simplified network is readily obtained using the transfer matrix method (Pannipitiya et al. 2010). The transmission coefficient \mathbf{T} of the SIS waveguide with the symmetrically placed parallel cavity can be obtained as (Matsuzaki et al. 2008).

$$\mathbf{T} = \left| 1 + \frac{Z_{SIS}}{Z_{Stub}} \right|^{-2} \exp\left(-\frac{L}{L_{SPP}}\right) \quad (3.6)$$

To illustrate the above transmission line model, for InSb waveguide we consider the parameters $G = 100\mu\text{m} = W$ for $L = 150\mu\text{m}$ (figure 3.5(a)) and $300\mu\text{m}$ (figure 3.5(b)). Figure 3.5 shows the comparison between the transmission line model (Impedance model) and the simulation. Eq 3.1 – 3.6 were used to calculate the transmission of the InSb waveguide with symmetrically placed stubs. For frequency range from 0.1THz to 1 THz, the waveguide devices reaches transmission minima at particular frequencies. For $G = 100\mu\text{m} = W$, $L = 150\mu\text{m}$ the device shows minima at 0.5THz and for $L = 300\mu\text{m}$ shows minima at 0.25THz and 0.75THz which agree well with the simulation model. Such impedance calculations can predict the transmission characteristics of the waveguide faster without any extensive numerical calculations compared with simulation.

3.4 InSb PLASMONIC DEVICE WITH TWO PAIRS OF STUBS

A waveguide device with two stub pairs is analogous to a coupled cavity optical resonator. It is expected to exhibit sharper resonance dips in the transmission profiles. Figure 3.6 shows the schematic of such a plasmonic device. The first stub is placed at the middle of the waveguide. The second stub is placed towards the output port at the distance P from the first stub. The two stubs have identical dimensions. The transmission characteristics of the device is studied by simulation and compared with that of the single stub device. The main results for this device are presented below.

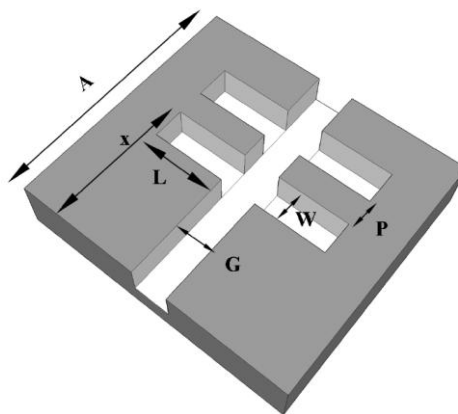


Figure 3.6: Schematic of the InSb waveguide with two stub pairs with $L = 150\mu\text{m}$, $W = G = 100\mu\text{m}$, Thickness of the waveguide $T = 1500\mu\text{m}$, $x = 600\mu\text{m}$, $A = 12000\mu\text{m}$, $P = 100\mu\text{m}$

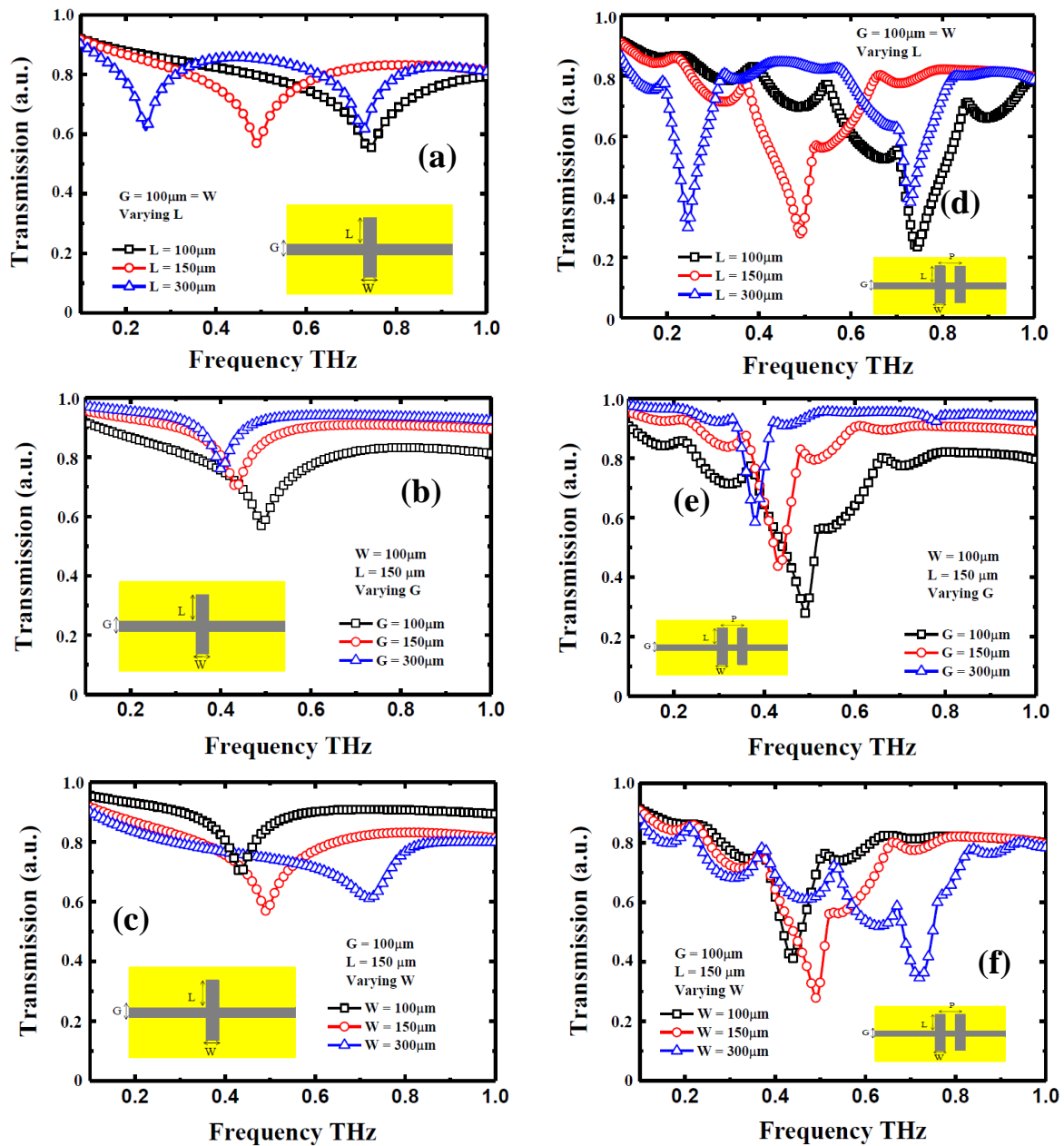


Figure 3.7: Simulated transmission characteristics of InSb THz Plasmonic waveguide device with stubs functioning as a resonator. **Single stub case:** varying (a) stub length L (b) waveguide width G (c) stub width W . **Double stub case** with $P = 100\mu\text{m}$: varying (d) stub length L (e) waveguide width G (f) stub width W .

We consider the InSb waveguide device having waveguide width $G = 100\mu\text{m}$, two identical pairs of stubs of width $W = 150\mu\text{m}$ separated by a distance $P = 100\mu\text{m}$. The stub length L , waveguide width G and stub width W are varied and their transmission characteristics were calculated. Figure 3.7 shows the results obtained through simulations using COMSOL Multiphysics. The graphs show sharper dips in the transmission at resonance frequencies for devices with double stub pair and high transmission over broad frequency ranges similar to the case of single stub pair device discussed in sec.3.2.2.

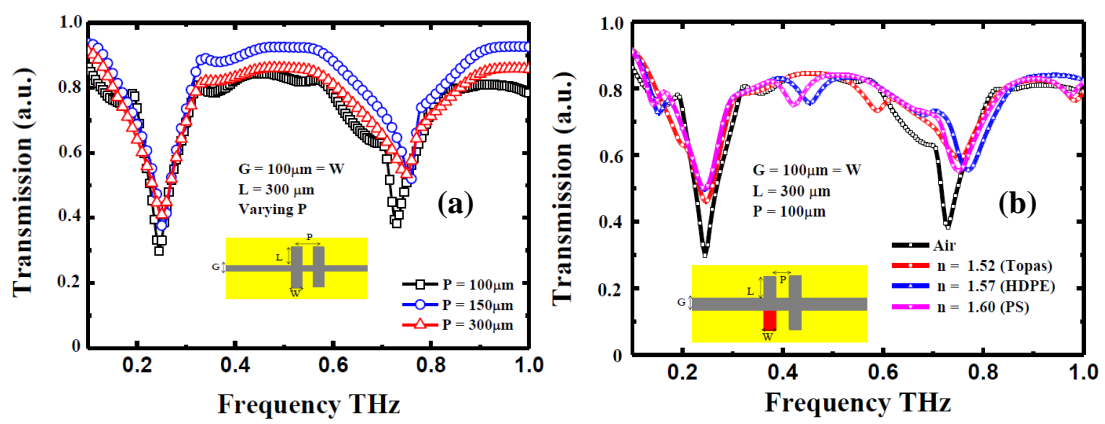


Figure 3.8 Simulated transmission characteristics of InSb THz Plasmonic waveguide device with double stubs with $G = 100\mu\text{m} = W$, $L = 300\mu\text{m}$ (a) by varying position of the stub (P) and (b) by changing the refractive index in one of the stub at $P = 100\mu\text{m}$ as shown in figure inset.

The transmission characteristics of InSb waveguide device with single stub (Figure 3.7(a, b & c)) and similar device with two pair of stubs (Figure 3.7(d, e & f)) are shown explicitly in the figure above. For the device with single pair of stub increasing the stub length L leads to large shift in the resonant frequencies and also to occurrence of multiple resonances within any frequency band as is clearly seen in figure 3.7a. The transmission minima which occurred at 0.745 THz for $L = 100\mu\text{m}$, shifted to 0.495 THz for $L = 150\mu\text{m}$ and for $L = 300\mu\text{m}$, minima occurred at two frequencies 0.245 THz and 0.725 THz within the frequency band $0.1\text{--}1.0\text{ THz}$. Similarly when the stub width W is increased, keeping G ($100\mu\text{m}$) and L ($150\mu\text{m}$) fixed, the resonance frequency shifted from 0.435 THz for $W = 100\mu\text{m}$ to 0.720 THz for $W = 300\mu\text{m}$

which is quite significant. However, as the waveguide width G is increased keeping W ($100\mu\text{m}$) and L ($150\mu\text{m}$) fixed, the resonance frequency shifts from 0.495 THz for $G = 100\mu\text{m}$ to 0.400 THz for $G = 300\mu\text{m}$. It is clear that changing the waveguide width G does not have any major effect on the transmission of the wave.

Figure 3.7(d, e & f) show transmission characteristics of InSb waveguide device with the inclusion of a second pair of stubs. As for the case of single stub pair, the transmission coefficient is computed for varying L , G and W . In this case too the same broad features, viz. frequency shift and occurrence of multiple resonances are seen. The major change with two stub pairs is that the resonance profiles are much sharper at the various resonant frequencies. The transmission minimum reduces from about 0.6 for single stub to ~ 0.2 for the two stub pair case. Thus, a device with double stub pair should be a much more sensitive filter device compared to a single stub device.

Figure 3.8a shows transmission characteristics of double stub InSb waveguide device for various spacing P between the stub pairs. The case $P = 100\mu\text{m}$ corresponds to that wherein the two stub pairs are located symmetrically along the waveguide; the distance of the first stub pair from the input end is the same as that of the second stub pair from the output end of the device. Further, the first stub is shifted towards the input end such that (i) $P = 150\mu\text{m}$ and (ii) $P = 300\mu\text{m}$. Varying the separation P between the stub pairs does not have any major effect on the signal transmission which is similar to the behaviour for varying waveguide width G .

Figure 3.8b shows the transmission properties of the double stub InSb waveguide device when one of the four stubs is loaded sequentially with three different dielectric materials. The Refractive Index (RI) of polyethylene cyclic olefin copolymer (Topas), polystyrene (PS) and high-density polyethylene (HDPE) are known to be 1.52 , 1.60 and 1.57 , respectively, and are almost constant in the THz frequency range (0.1 - 2 THz) (Cunningham et al. 2011). When any one of these material is loaded into the device, a measurable frequency shift of about 0.72 to 0.75 THz is seen in the resonance dip at the higher frequency.

Most significant change is the appearance of an additional resonant frequency at 0.586 THz when $RI = 1.52$. As the RI increases there is a shift in this resonant frequency to 0.461 for $RI = 1.57$ and to 0.419 for $RI = 1.60$. When a sample material is placed in one of the stubs, the presence of the sample can be detected by analyzing the transmission characteristics of the device at THz frequencies. Such criteria can be utilized to model the THz InSb waveguide device with double stub pair to function as a good material sensor similar to the single stub pair case.

3.5 CONCLUSIONS

In summary the transmission characteristics of InSb THz waveguide device with stubs were studied by simulation using COMSOL Multiphysics and Ansoft HFSS softwares. The stubs along the waveguide act as resonant cavity, thereby, making the device to function as a narrow band filter. The geometry of the device decides the resonant frequency. The transmission characteristics of the devices were investigated for varying stub length (L) keeping the waveguide width constant at $G = 1000 \mu\text{m}$. The transmission minimum occurred at 0.236THz for $L = 450\mu\text{m}$. For $L = 750\mu\text{m}$ minima occurred at two frequencies 0.218THz and 0.276THz. These two minima got slightly shifted to 0.213THz and 0.28THz when L was further increased to $1000\mu\text{m}$. Similarly the devices were investigated for varying waveguide width (G) and fixed stub length $L = 1000 \mu\text{m}$. The device showed transmission minimum at 0.219THz for $G = 450\mu\text{m}$, at 0.238THz and 0.292THz for $G = 750\mu\text{m}$ and for $G = 1000\mu\text{m}$ the minima shifted to 0.213THz and 0.28THz. Thus, by choosing the size of G or L , the device can be designed to possess a single or multiple resonance frequencies. These studies are useful in designing the devices for actual experimentation. The transmission characteristics for the InSb plasmonic devices obtained by simulation using COMSOL were compared with analysis based on equivalent Transmission Line model. The analytical model is based on the similarity of waveguide devices having stubs with the standard transmission lines with lumped impedances, including interference between the incident wave and the wave reflected from the stub. Simulation results, using COMSOL, for the InSb plasmonic waveguide device for

different stub configurations showing transmission minima at particular frequencies agree well with the results obtained using transmission line model. This analytical model can predict the transmission spectra of the waveguide device much faster compared to the COMSOL simulations. Finally, the improvement in the filtering performance of the device with the double stub was also studied by varying L, G, W and P. The transmission characteristics was similar to single stub case with much sharper resonance profile at resonant frequency and the minimum value of transmission reduces from about 0.6 for single stub to about 0.2 for the two stub pair case. Transmission of InSb waveguide device with double stub was studied to sense the change in refractive index in one of the stubs. Appearance of an additional resonance frequency and shift in this resonant frequency as the RI in the stub changes can be utilized in InSb waveguide device with double stub to function as a better material sensor similar to the single stub.

CHAPTER 4

FABRICATION AND CHARACTERIZATION OF InSb THz PLASMONIC WAVEGUIDE DEVICE

Abstract

This chapter presents details of the fabrication and characterization of the InSb devices at Terahertz frequencies. The transmission characteristics of the devices was investigated numerically and compared with experimental measurements at terahertz (THz) frequencies employing Time Domain Spectroscopy (TDS) techniques. The waveguide devices were fabricated by laser micromachining. The experimental results were seen to match with the simulation results.

4.1 INTRODUCTION

THz Plasmonic devices have sub-wavelength dimensions, and are faster, efficient and are well suited for incorporation into a lab on chip. They are opening up new avenues to develop novel device applications in THz technology (Dragoman et al 2008). THz devices studied so far include metal based parallel plate waveguide with resonant cavities, (Chen et al 2013, Reichel et al 2014), fibre based dielectric waveguide (You et al 2012), corrugated waveguide (Kumar et al 2011), metallic meshes (Hasebe et al 2012), etc. In Plasmonic devices, the electromagnetic waves propagate as surface waves. Consequently, the devices can have sub-wavelength dimensions. The other important feature is that, the electric field of the wave, and hence, the wave energy is strongly localized close to the semiconductor-dielectric interface. Therefore, such devices can support SPPs at the interface between dielectric and metal or semiconductor, with low propagation loss and low dispersion at terahertz frequencies (Wächter et al 2007, Steven 2014). In a waveguide made of Indium Antimonide (InSb), one can generate SPP at THz frequencies at the semiconductor-dielectric interface (Vincenzo et al 2010, Paul et al 2007) as discussed in chapter 2.

In this chapter we describe the fabrication technique used for the planar THz Plasmonic waveguide device, made using InSb. Of the various methods tried for fabricating the devices, laser micro-machining on InSb pellets was seen to be a simple and fast method. InSb waveguide devices, with and without stubs, were fabricated and THz Time Domain Spectroscopy (TDS) technique was used to experimentally measure the transmission characteristics of the devices. Simulated and measured transmission characteristics of the device were compared and assessed for sensing applications.

4.2 FABRICATION AND CHARACTERIZATION

Indium (99.99% purity) and Antimony (99.99% purity) powders were mixed in the ratio 1:1 and grounded using a mortar and pestle to get a fine powder. The powdered sample was placed in a quartz crucible and heated under vacuum at 100⁰C for 15 minutes and then cooled down. The heat treated sample was again ground and heated to a higher temperature at 120⁰C for 15 minutes to form InSb. This process was repeated thrice. The powder X-Ray Diffraction (XRD) analysis confirmed the synthesis of InSb with prominent peaks (Figure 4.1a). The typical EDAX spectrum is also shown in figure (4.1b). The analysis confirmed the stoichiometry of the synthesized InSb with the In: Sb ratio 50.48 : 40.42. Finally, the processed InSb powder was cast into square pellets of dimensions 1.2cm x 1.2cm x 2mm using hydraulic pellet press (Figure 4.1c).

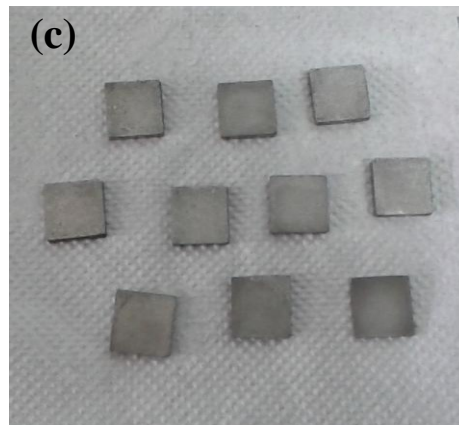
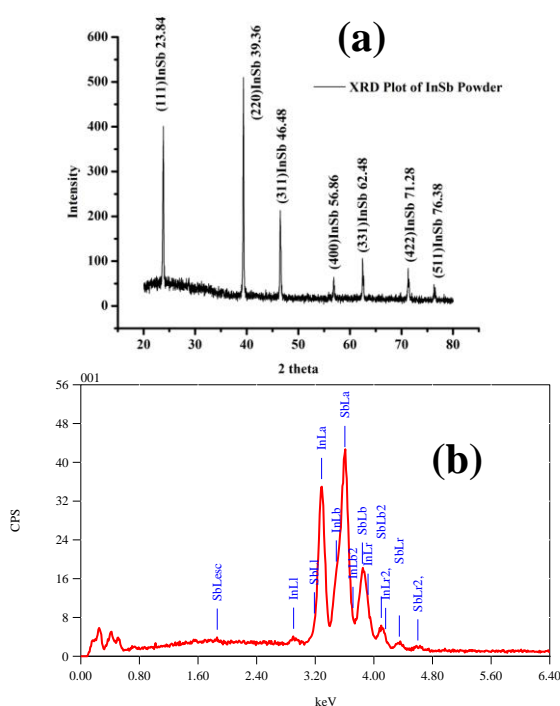


Figure.4.1 (a) XRD spectra of powder InSb, (b) EDAX spectra of powder InSb, (c) Casted InSb pellets of dimensions 1.2cm x 1.2cm x 2mm

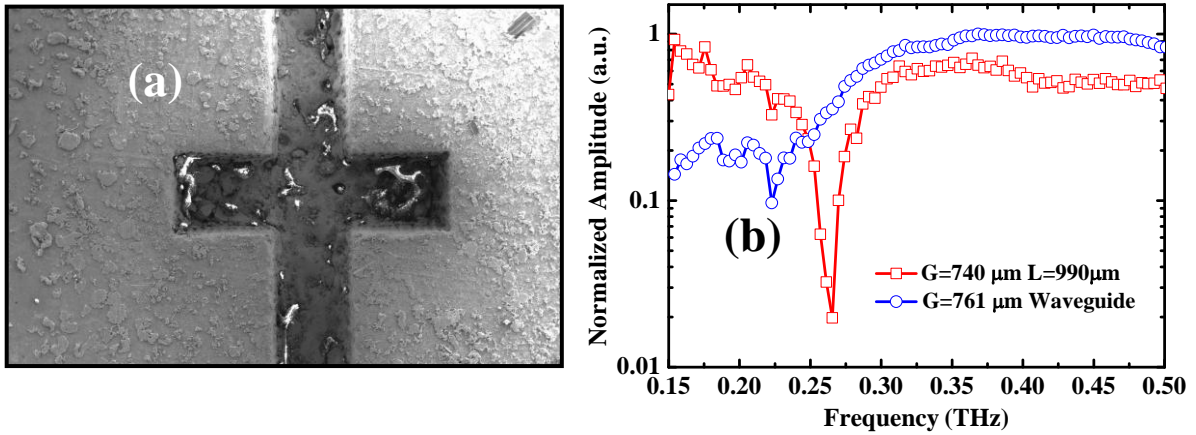


Figure.4.2: (a) SEM image of the fabricated device showing top view. (b) Measured transmission spectra of the THz pulse for InSb waveguide with stub of $G = 740\mu\text{m}$ and $L = 990\mu\text{m}$ showing T_{\min} at 0.265 THz, and InSb waveguide without stub with $G = 761\mu\text{m}$.

The prepared InSb pellets were dipped in the etchant HF: H_2O_2 (in the ratio 10:1), suitable for InSb (Clawson 2001), for 10 minutes at room temperature to remove oxides formed on the surface. Laser micro-machining was employed for creating trenches on the pellet by laser ablation of the material using a CW Fibre Laser, generating 30 Watts output power at a wavelength of 300 nm. The laser beam had a Gaussian intensity profile which could be focused to a single spot. The resulting rectangular grooves made on one face of the InSb pellet constituted the waveguide and the two stubs, oriented perpendicular to the waveguide section.

InSb devices with different waveguide widths and stub lengths were fabricated to investigate the dependence of the resonance frequency and the transmission characteristics of the device on the device dimensions. Figure 4.2a shows the SEM image of one fabricated InSb waveguide device.

For a detailed investigation of the transmission characteristics, devices with following parameters were fabricated

Table I. Device parameters of the fabricated InSb waveguide device

S. No	1.	2.	3.	4.	5.
G(μm)	495	630	740	736	740
L(μm)	945	988	990	1524	1894

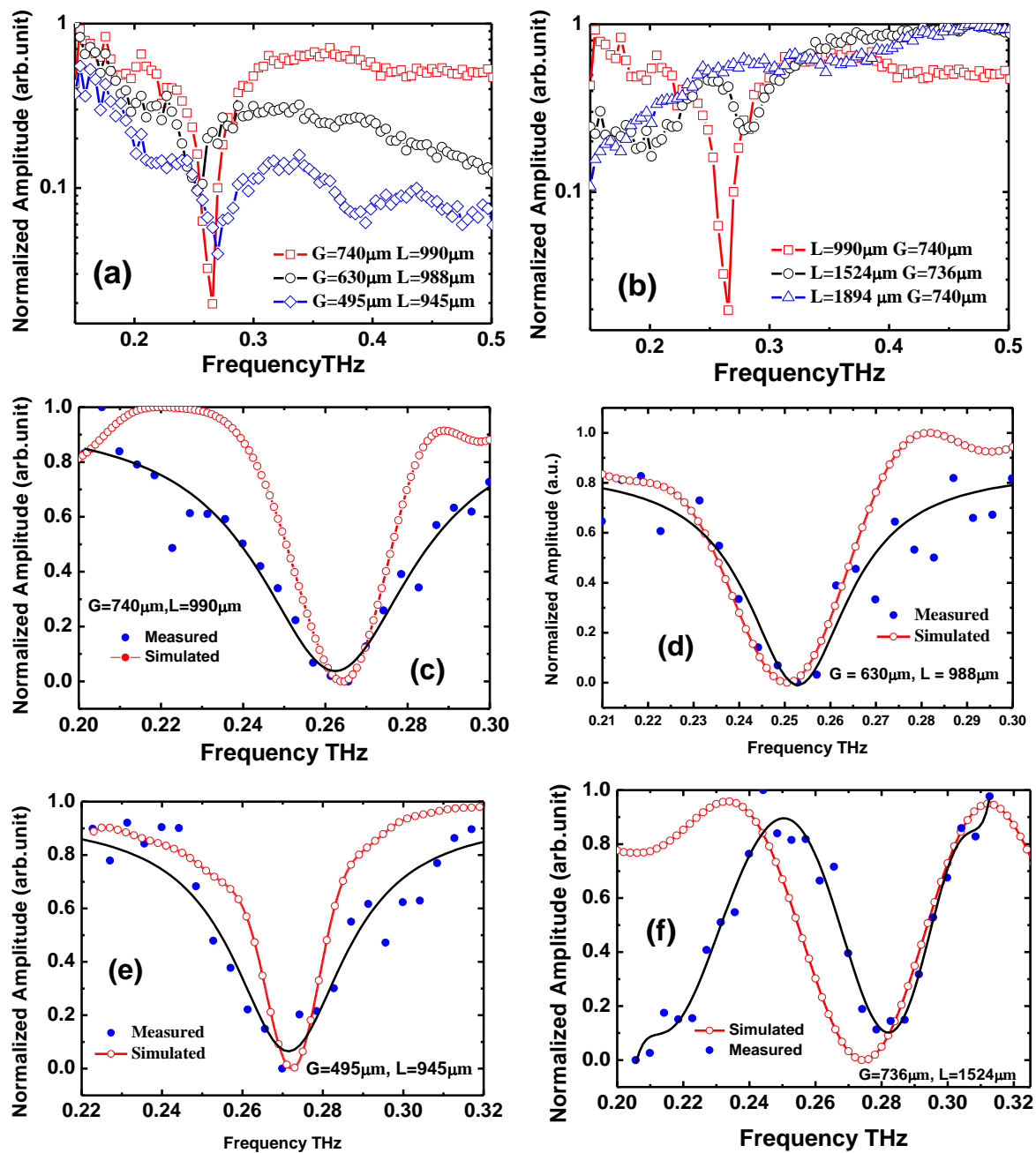


Figure 4.3: (a– b) show the measured transmission spectra of the THz pulse for different waveguide-widths and stub-widths. Plots (c) to (f) show the comparison of the simulated and the measured spectra of the transmitted THz radiation. All the spectra shown have been normalized by the amplitude spectra obtained without mounting the device on the holder.

A standard THz-TDS set-up was used to measure the transmission characteristics of the InSb devices. The setup consists of a femtosecond (fs) Ti:Sapphire laser generating 10 fs pulses at a wavelength of 800nm and at a pulse repetition rate of 76MHz. The optical pulses from the laser are focused on to a biased LT-GaAs based photoconductive antenna. Each pulse creates an electron-hole pair and subsequent acceleration of these carriers by the bias field generates a nearly single cycle electromagnetic pulse of THz radiation.

A pair of off-axis parabolic mirrors was used to focus the THz radiation onto the input port of the device mounted on a holder. The guided modes exit from the output port (Figure.4.2a) and the transmitted THz signal was collected by another pair of parabolic mirrors and detected by a ZnTe based electro-optic detection setup. Waveforms of the THz radiation transmitted through the devices without stubs and with stubs were acquired and their Fast Fourier Transforms (FFT) computed.

The FFT spectra obtained with the device mounted on the holder was normalized by dividing it with the spectra obtained without the device on the holder. This ratio is defined as normalized amplitude. Figure 4.3 shows the simulated and measured amplitude transmission of the devices. The transmission shows a sharp dip at a certain frequency (termed resonant frequency) for certain values of G and L. The resonant frequencies for the various devices fabricated are shown in Table II. The measured results show good agreement with the simulated ones. The deviations in the measured and simulated frequencies could be due to roughness created in the waveguide/stub walls during the laser micromachining process.

Dimensions of the input aperture, with $D = 1.8$ mm, determines the cut-off frequency to be $F_c = 0.083$ THz ($F_c = c/2D$, c = speed of light in vacuum) of the waveguide. This gives rise to a lowest order TM SPP mode, called the plasmonic mode (Zhu et al 2011) with highly confined electric field in the waveguide channel region of width (G) and evanescently decaying field in the semiconductor region adjoining the channel walls (Vincenzo et al 2010).

Table II. Comparison of the measured and simulated resonant frequency values.

G(μm)	L(μm)	Measured (THz)		Simulated (THz)	
		γ_0	$\Delta \gamma$	γ_0	$\Delta \gamma$
495	945	0.269	0.021 (± 0.004)	0.249	0.019
630	988	0.252	0.026 (± 0.007)	0.245	0.031
740	990	0.265	0.036 (± 0.003)	0.268	0.026
736	1524	0.278	0.031 (± 0.005)	0.275	0.039

γ_0 = Resonance frequency, $\Delta \gamma$ = FWHM

Above the cut off frequency the device shows several transmission maxima and minima as a function of frequency. This can be attributed to the interference between the forward propagating wave and the wave reflected from the stub (Jin et al. 2013).

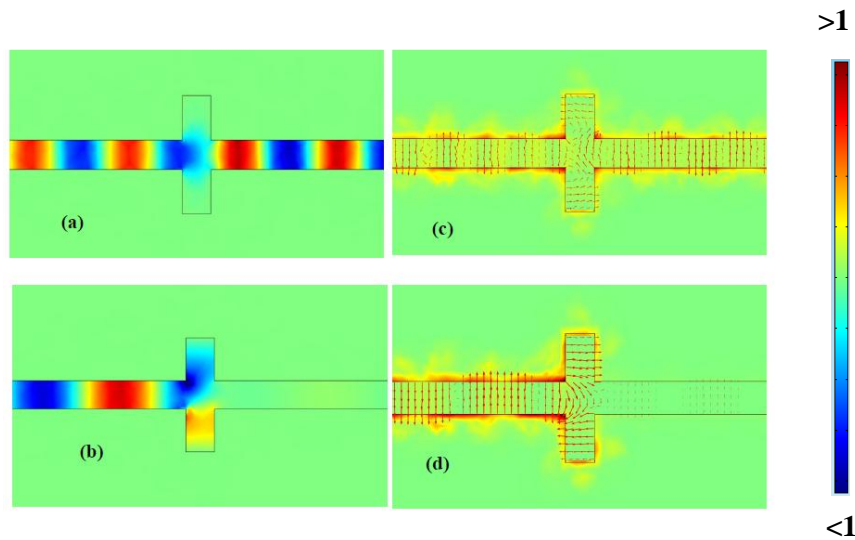


Figure 4.4: (a & b) : Simulated Electric field distribution in the InSb THz Plasmonic device for wave frequency of 0.3 THz and 0.249 THz, respectively; (c & d) :Electron charge density distribution at the semiconductor-air interface along the waveguide and the stub at the frequencies of 0.3 THz and 0.249 THz, respectively. The device dimensions are $G = 495\mu\text{m}$, $L = 945\mu\text{m}$.

Figure 4.4(a) shows the electric field distribution at a frequency of 0.3 THz and represents maximum signal transmission. The same device shows transmission minimum at 0.249 THz as seen in figure 4.4 (b). Figure 4.4 (c and d) show the corresponding electron charge density distribution, at the semiconductor-air interface along the waveguide and the stub, for maximum and minimum transmission, respectively.

Figure 4.5 shows the “Transmission Map” depicting the transmission characteristics of the device with the guided-wave frequency (in THz) and the waveguide width G (in μm) as two parameters. The green stripes represent regions of very low signal transmission. Thus, for G value of about $300\mu\text{m}$, the transmission shows sharp dip at frequencies 0.226 THz (I Mode) and 0.376 THz (II Mode). At these parameters the wave electric field increases strongly inside the stub and very little energy is transmitted out of the device. At other frequencies the signal transmission is very high and the electric field in the stub is negligible (Mendis et al. 2009) as is also evident from figure 4.3.

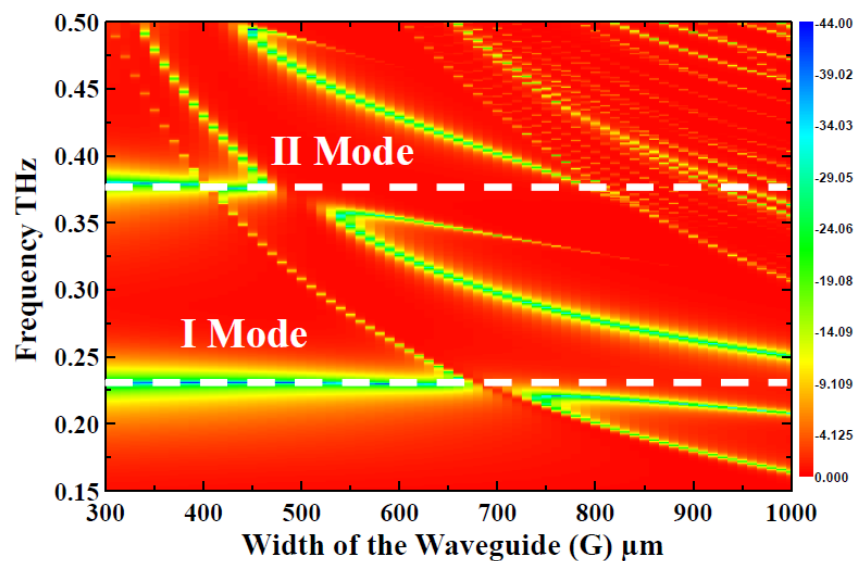


Figure 4.5: Finite element method based transmission coefficient (in dB) at THz frequency for various gaps. This 2D image is for InSb waveguide with $L= 1000 \mu\text{m}$ and $G = W$ with dashed lines showing the resonant modes inside the stub leading to transmission minima.

It is also clear from figure 4.5 that the device could be designed to operate at a chosen resonance frequency, at which the transmission exhibits a sharp dip. Further, frequency tunability of the device is also possible since the carrier concentration of InSb can be altered by electrical or optical methods. This modulates the frequency dependent permittivity of InSb leading to changes in the transmission characteristics of the device.

4.3 CONCLUSIONS

In conclusion, we have investigated experimentally the THz transmission characteristics of InSb plasmonic waveguide devices with stubs and shown that they function as a frequency selective filter. InSb waveguide devices were fabricated with the following dimensions, $G = 495 \mu\text{m}$, $L = 945 \mu\text{m}$; $G = 635 \mu\text{m}$, $L = 988 \mu\text{m}$; $G = 740 \mu\text{m}$, $L = 990 \mu\text{m}$; $G = 736 \mu\text{m}$, $L = 1524 \mu\text{m}$. The transmission minimum occurred at 0.269THz, 0.252THz, 0.265THz, and 0.278THz respectively, which agree well with the simulation. The transmission resonance dip of the device shows a shift as the width of the waveguide G and the stub length L is varied. At those resonance frequencies there is a strong interaction of propagating electric field \vec{E} with the stub, resulting in low signal transmission of the device. At other frequencies the devices show high transmission. The effect of varying G and L was studied experimentally which leads to difference in confining the electric field inside the stub and shifts the resonance frequency. The amplitude difference can be correlated to the coupling efficiency between the incident THz signal and the cross sectional area of waveguide input port. Results from finite element method simulation using COMSOL Multiphysics show similar trend in the resonant frequency of the designed InSb waveguide device with stubs. This resonance feature of the device was used to sense the presence of protein–water (BSA-W) mix and Polystyrene (PS) dissolved in toluene at different concentrations. The ability of the device to work as a sensitive biosensor is discussed in the next chapter.

CHAPTER 5

InSb WAVEGUIDE DEVICES AS MATERIAL SENSORS

Abstract

This chapter demonstrates the possibility of employing the InSb plasmonic waveguide device, designed to operate at terahertz (THz) frequencies, for sensing materials. For a waveguide width of 740 μm and stub length of 990 μm , a transmission minimum is seen to occur at 0.265 THz. We investigated the capability of the device to sense protein molecule Bovine serum albumin (BSA) and polystyrene, dissolved in toluene, loaded into the stubs. The consequent change in the refractive index in the stubs alters the transmitted signal intensity. Our results show that, a change in the concentration of the loaded sample even by 1mol/L, leads to measurable change in the transmission coefficient close to the resonant frequency of the device. Thus, these plasmonic devices operating at THz frequencies show promising potential as chemical and bio sensors.

5.1 INTRODUCTION

Terahertz technologies have opened up new domains in Sensor development. Researchers are now equipped with new tools for qualitative as well as quantitative sensing of various materials including chemicals and biological materials. This interest in using terahertz radiation for detecting materials is due to the fact that radiation at these frequencies excites the vibrational and rotational energy levels in the complex molecules, which turn out to be characteristic signatures of the molecules.

The accurate detection of chemical and biological substances in minute quantities has been a major goal in THz sensing in the past few years. A wide variety of sensing strategies have been developed to provide high sensitivity, reusability, portability, miniaturization, low cost for mass production, small sample volume and ease of use. These features constitute desirable requirements for any sensor. THz sensing devices like PPWG (Laman et al. 2008), THz antennas (Berrier et al. 2012), split ring

resonators, metamaterials (Singh et al 2014), Polymer THz fiber (You et al. 2012), are a few of the THz devices developed for sensing applications.

Among the various options, devices having a resonant cavity have proved to be the most promising. A Parallel Plate Wave-Guide (PPWG) with a resonant cavity, forming a part of a lab-on-chip device, was demonstrated to function as a highly sensitive refractive index sensor with a sensitivity of 91.25 GHz/RIU (Mendis et al 2009). A THz metamaterial device, consisting of symmetric split ring resonators, was exploited as ultrasensitive refractive index sensor, possessing a sensitivity of 36.7 GHz/RIU and 23.9 GHz/RIU when Fano and Quadrupole resonances, respectively, were excited (Singh et al 2014). THz antenna (Berrier et al 2012) was used to detect bacteria with high sensitivity. These THz sensors can sense ultra-thin (a few nanometer thick) molecular layers [John et al 2008) and a few femto-moles of DNA molecules (Nagel et al 2002). Recently, a THz metamaterial absorber with cross shaped elements was demonstrated as a sensor showing enhanced sensitivity compared to planar metal-surfaces (Longqing et al 2015). Thus, resonant structures are seen to have a big advantage over planar devices and, hence, can be integrated with conventional electronics and other micro-sized devices to function as compact sensor modules.

This chapter focuses on demonstrating the sensing capability of InSb Plasmonic THz waveguide device with stub. Two types of materials, a protein and a polymer, have been chosen for our experiments. In our Plasmonic device, as discussed in the previous chapters, the electromagnetic waves propagate as surface waves. The other important feature is that, the electric field of the wave, and hence, the wave energy is strongly localized close to the semiconductor-insulator interface. This enables a strong interaction of the wave with any material loaded into the device, leading to significant changes in the transmission of the THz signal.

The two materials under investigation in this thesis are,

- Protein - Bovine Serum Albumin (BSA)
- Polymer - Polystyrene dissolved in Toluene

5.2 BOVINE SERUM ALBUMIN

Bovine Serum Albumin (BSA) (Markelz et al. 2000) is a well studied protein molecule. Hence it is chosen to study the sensing characteristics of the InSb waveguide device. Experiments were performed to measure the THz transmission of the device when loaded with a solution of the protein molecule BSA in deionised water at various concentrations.

The prepared BSA-water (BSA-W) solution was dropped, using a common syringe, into the stubs of the InSb device having dimensions $W = G = 740 \mu\text{m}$, $L = 990 \mu\text{m}$. THz- TDS measurement was carried out as described in chapter 1 & 4.

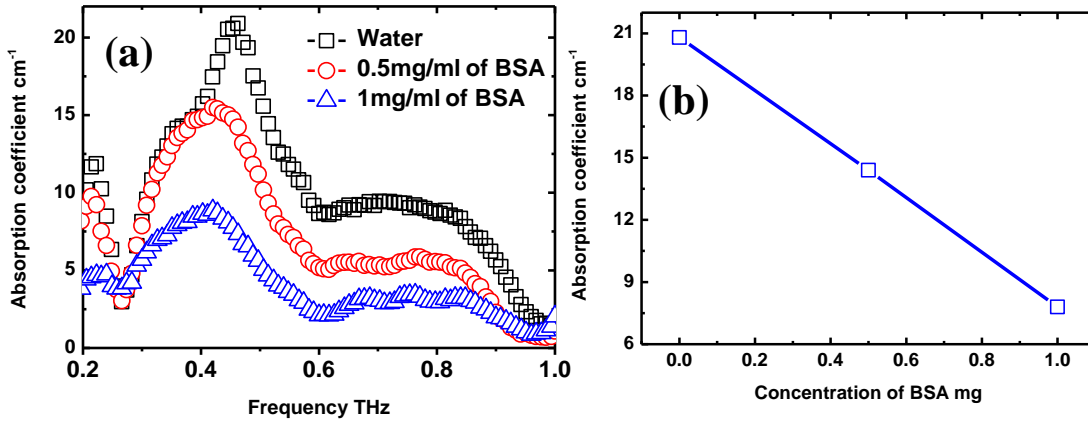


Figure. 5.1(a) Calculated Absorption coefficient of the BSA-Water solution, loaded into the stub of the plasmonic device, from the normalized amplitude measured by the THz-TDS technique. **(b)** Absorption coefficient versus concentration of BSA. Slope of the linear fit

gives a sensitivity of $\sim 13 \frac{\text{cm}^{-1}}{\text{mg / ml}}$.

The transmitted amplitude measured with just deionised water in the stub is considered as the reference field amplitude E_{ref} . Measurements were then carried out by loading the device with 0.5mg/ml and 1mg/ml of BSA concentrations and the measured field amplitude is E_{sample} . Before each measurement using BSA-W sample, transmission of THz beam in the InSb device with the empty stub and with stub filled with deionised water (E_{ref}) were measured to ensure consistency in the measurements.

The effective absorption coefficient (α_{eff}) as a function of frequency (ω) of the measured spectra was defined as (Kitagawa et al 2006),

$$\alpha_{eff}(\omega) = -\frac{1}{W} \ln \frac{E_{sample}(\omega)}{E_{ref}(\omega)} \quad (5.1)$$

where W ($\sim 740\mu\text{m}$) is the width of the stub, called as the sensing length, E_{sample} and E_{ref} are the Fourier transformed spectra corresponding to BSA and deionized water. Figure 5.1(a) shows $\alpha_{eff}(\omega)$ calculated from the measured data when the device was loaded first with water and next with BSA solution of concentration 0.5mg/ml and 1mg/ml. As the concentration of BSA increases, the number of absorbing water molecules decreases for a fixed quantity of the solution, leading to decrease in $\alpha_{eff}(\omega)$. The observed decrease in $\alpha_{eff}(\omega)$ with the increasing concentration of the BSA molecule is consistent with results reported (Kitagawa et al 2006, Paul et al 2008).

We determined the sensitivity of the sensor by noting the decrease in the absorption coefficient with increasing concentration of BSA. The plot of the decrease in the absorption coefficient, at 0.45 THz, versus the concentration of BSA is shown in the figure 5.1(b); the graph for water corresponds to zero concentration of BSA. The data points indicate a linear fit over the range of concentration used in our experiments. The slope of the graph yields a sensitivity of about $\sim 13 \frac{cm^{-1}}{mg/ml}$. Thus, a minute change in the concentration of BSA shows prominent change in the absorption coefficient. This characteristic of our device demonstrates the sensing capability of the device and its potential as a biosensor.

Plasmonic stub-waveguide device sensors also show a shift in the resonance frequency when loaded with material media. However, within the limitations of our experiments, such frequency shifts were smaller than ~ 0.001 THz and, further investigations are underway to explore this aspect.

5.3 POLYSTYRENE DISSOLVED IN TOULENE

Polystyrene is a polymer, widely used as a packaging material and for making disposable containers. Such materials have promising applications in THz Optics for making components such as lenses, windows, beam-blocks and waveguides (Cunningham et al. 2011). Sensing characteristics of our device was investigated by

filling one of the stubs with a solution of polystyrene in toluene at different concentrations. The solutions, thus prepared, were colourless, viscous in nature and had a refractive index almost constant in the frequency range 0.1 to 5 THz (Cunningham et al. 2011). In our experiments, a few millilitres of the solution were dropped into one of the two stubs in the device and the transmission of THz waves through the device was measured.

The THz time domain signal of the device was measured (Figure.5.2 (a)) in the following three steps in sequence

1. Measurement without filling the stubs with any liquid or sample $[E_A(\omega)]$
2. Measurement after filling one of the stubs (inset in Fig. III (b)) of the waveguide with Toluene $[E_T(\omega)]$
3. Measurement after filling one of the stubs with the sample solution (PS) $[E_P(\omega)]$

The symbols in the brackets denote the corresponding FFT spectra.

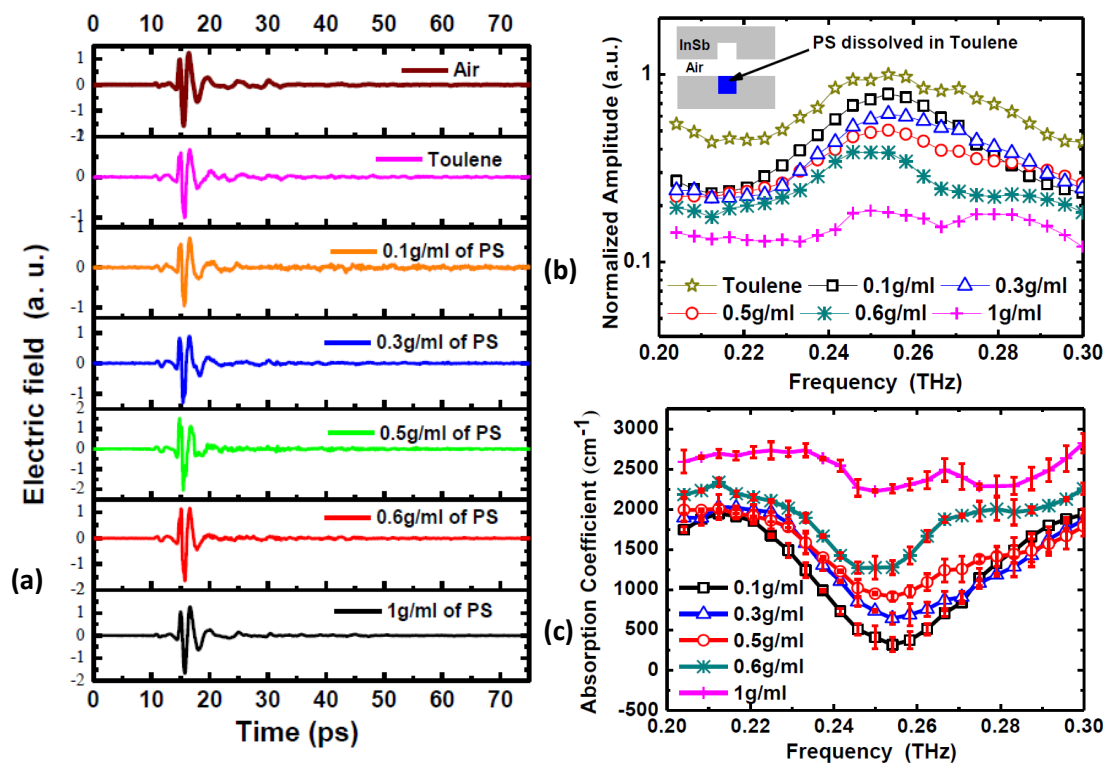


Figure.5.2 (a) Measured time-domain transmitted electric field signals for the device loaded with polystyrene solutions (PS) at various concentrations , (b) Corresponding computed THz transmission spectra, (c) Variation of absorption coefficient of the samples with frequency.

The transmission measurements were repeated for each sample to ensure consistency. The quantities $E_T(\omega)/E_A(\omega)$ for pure toluene and $E_P(\omega)/E_T(\omega)$ for solution of polystyrene at different concentrations are shown in (Figure.5.2 (b)).

Figure.5.2 (b) indicates a monotonic decrease, over a significant frequency range, in the transmission of the THz wave with increasing concentration of polystyrene in toluene. The effective absorption coefficient (α_{eff}) as a function of frequency of the measured spectra was calculated as shown in Eq. 5.1, where $W \sim 750 \mu\text{m}$ is the width of the stub.

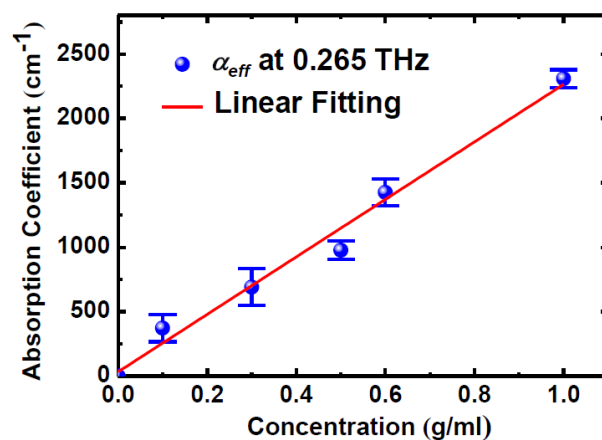


Figure 5.3 Absorption coefficients versus concentration of PS at the resonant frequency of 0.265 THz showing a linear behaviour. The slope of the graph yields a sensitivity of $\sim 2200 \frac{\text{cm}^{-1}}{\text{g/ml}}$.

(Figure.5.2 (c)) shows the variation of $\alpha_{eff}(\omega)$ with frequency at different concentrations of polystyrene, as calculated from the data shown in (Figure.5.2 (c)). When the sample material with different permittivity was placed inside one of the stub, the propagating THz wave experiences a dielectric loss in the stub. Due to the resonance characteristics of our device, the change in the transmission coefficient turns out to be very sensitive to varying concentration of polystyrene.

Figure.5.3 shows α_{eff} at 0.265 THz (for $G = 740\mu\text{m}$, $L = 990\mu\text{m}$) for different concentrations of the solution. It is seen that absorption of the THz wave increases with increase in the concentration of polystyrene in the solution. The sensitivity of

our measurement, obtained from the slope of the graph, is $\sim 2200 \frac{cm^{-1}}{g/ml}$. It is clear that,

exploiting the resonant nature of the device to enhance the wave electric field in the stubs is a simple and a promising method to sense the presence of a minute quantity of a polymer.

5.4 CONCLUSIONS

In conclusion, we have shown that an InSb plasmonic waveguide device can detect the presence of minute quantity of materials with high sensitivity. Our device functions as a resonant structure, showing minimum transmission at a particular frequency in the THz range. Loading one of the stubs with the sample material reduces the transmission coefficient of the device for THz waves of frequency close to the resonant frequency. A minute change in the concentration of the solution, changes the effective refractive index of the stub filled with the sample material. Dissolving protein molecules in water, in bulk quantity and studying their THz properties is a formidable task. Using only a micro litre quantity of BSA-W solution in our device and be able to detect the BSA-W concentrations with the sensitivity $\sim 13 \frac{cm^{-1}}{mg/ml}$ is a very substantial improvement over this problem. Similarly, the transmitted amplitude reduces as the concentration of polystyrene in toluene increases with the sensitivity of $\sim 2200 \frac{cm^{-1}}{g/ml}$. Even a change of 1mol/L in the concentration can be measured using our device. This characteristic of our device demonstrates its sensing capability and its potential as a good sensor. The device is simple to fabricate, has a small foot-print and it is possible to incorporate multiple plasmonic devices into a single sensor system in a lab-on-chip environment.

CHAPTER 6

SUMMARY AND CONCLUSIONS

6.1 THz InSb WAVEGUIDE DEVICE WITH STUB AS RESONANT STRUCTURE

- ❖ THz Plasmonic waveguide devices were designed and simulated to operate in the frequency domain 0.1-1.0 THz.
- ❖ Frequency dependent permittivity of InSb was modelled using Drude free electron model.
- ❖ COMSOL Multiphysics and Ansoft HFSS, FEM based simulation tools, were used to solve the EM boundary value problem and to model and simulate the designed SIS waveguide device.
- ❖ The Effective Index method has been employed to study the surface plasmon propagation in the InSb channel waveguide of sub-wavelength width.
- ❖ Surface plasmon propagation and the filtering properties of InSb waveguide device, coupled to single and two pair of stubs, which functions as a resonator at THz frequencies were numerically studied.
- ❖ These waveguide devices with stubs resonate at particular discrete frequencies called the resonant frequencies and transmit all other frequencies.
- ❖ The major change with two stub pairs is that the resonance profiles are much sharper at the various resonant frequencies. Thus, a device with double stub pair should be a much more sensitive filter device compared to a single stub device.
- ❖ The resonant nature of the devices was proved analytically using the microwave transmission line theory by modelling the waveguide device as an equivalent RLC circuit following the work of Pannipitiya et al. 2010.
- ❖ THz InSb waveguides were fabricated on InSb pellets using laser micromachining.

- ❖ The transmission characteristics of the fabricated waveguide device were studied experimentally using THz – TDS. The devices showed resonance dip and also a shift as width of the waveguide G and the stub length L is varied.
- ❖ At resonance frequencies there is a strong interaction of propagating electric field with the material present in any stub, resulting in large changes in the transmission coefficient of the device.

6.2 THz InSb WAVEGUIDE DEVICE AS MATERIAL SENSOR

- ❖ The resonance feature of the device was exploited to study the suitability of the device to function as a sensitive chemical sensor using (a) protein - Bovine Serum Albumin (BSA), (b) polymer - Polystyrene dissolved in toluene as samples.
- ❖ The chemicals introduced inside the stub of the InSb waveguide device altered the permittivity of the medium, thereby changing the transmission close to the resonant frequency of the device.
- ❖ Absorption coefficient calculated from the transmission measurements clearly indicated the presence of chemical inside the stub making InSb waveguide a sensitive chemical sensor.
- ❖ Dropping only a micro litre quantity of sample in the stub resulted in detecting BSA concentrations with the sensitivity $\sim 13 \frac{cm^{-1}}{mg/ml}$ and polystyrene dissolved in toluene with the sensitivity of $\sim 2200 \frac{cm^{-1}}{g/ml}$.
- ❖ Loading one of the stubs with the sample material reduces the transmission coefficient of the device for THz waves of frequency close to the resonant frequency. Even a change of 1mol/L in the concentration can be measured using this device.
- ❖ Clearly InSb THz plasmonic waveguide is a simple and flexible device for sensing application and has a possibility of incorporating multiple sensors into a single device for a lab on chip environment.

6.3 SCOPE FOR FUTURE WORK

The present research investigations can be further extended in the following directions,

- Present investigations focused on using intrinsic semiconductor InSb for THz plasmonic devices. This can be extended by using doped InSb, Si, Ge or other semiconductors whose plasma frequency fall in the THz region.
- Transmission characteristics of InSb waveguide device can be made tuneable by varying the carrier concentration of InSb thermally or optically.
- The studies presented here were mainly focused on InSb waveguide device with single stub. Only simulations were carried out for double stub case. Experimental investigations on the transmission characteristics of InSb waveguide device with double stub pairs can be carried out.
- Transmission coefficient of few more chemicals can be measured using the InSb waveguide device to examine the suitability of the device as a chemical sensor.

REFERENCES

- ♣ Auston D. H., Johnson A. M., Smith P. R., and Bean J. C. (1980). “Picosecond optoelectronic detection, sampling, and correlation measurements in amorphous semiconductors.” *Applied Physics Letters* 37, 371.
- ♣ Auston D. H., Cheung K. P., and Smith P. R. (1984). “Picosecond photoconducting Hertzian dipoles.” *Applied Physics Letters* 45, 284 (1984).
- ♣ Barnes William L., Alain Dereux, Thomas W. Ebbesen (2003). “Surface plasmon subwavelength optics.” *Nature*, Vol. 424, 824-830.
- ♣ Berini P. (2000). “Plasmon-polariton waves guided by thin lossy metal films of finite width: bound modes of symmetric structures.” *J. Phys. Rev. B* 61, 10484-10503.
- ♣ Berini P., Stohr A., Wu K., Jager D. (1996). “Normal mode analysis and characterization of an InGaAs/GaAs MQW field-induced optical waveguide including electrode effects.” *J. Lightwave Technology*. 14, 2422-2435.
- ♣ Berrier A, M. C. Schaafsma, G. Nonglaton, J. Bergquist, and J. G. Rivas (2012). “Selective detection of bacterial layers with terahertz plasmonic antennas ” *Optics Express*, 3, 11, 1–4.
- ♣ Bozhevolnyi Sergey I., Valentyn S. Volkov, Eloïse Devaux, and Thomas W. Ebbesen (2005). “Channel Plasmon-Polariton Guiding by Subwavelength Metal Grooves.” *Phys. Rev. Lett.* 95, 046802.
- ♣ Bozhevolnyi S.I, Davoyan A, Shadrivov I.V, , Kivshar Y.S (2010). Backward and forward modes guided by metal-dielectric-metal plasmonic waveguides. *J. Nanophotonics*. 0001;4(1):043509-043509-10.
- ♣ Burton, F.A.; Cassidy, S.A. (1990). “A complete description of the dispersion relation for thin metal film plasmon-polaritons.” *J. Lightwave Technology* , vol.8, no.12, pp.1843,1849.
- ♣ Chen H.T., W. J. Padilla, J. M. O. Zide, A. C. Gossard, A. J. Taylor, and R. D. Averitt (2006). “Active terahertz metamaterial devices.” *Nature* 444(7119), 597–600.
- ♣ Chen H.T, H. Lu, A. K. Azad, R. D. Averitt, A. C. Gossard, S. A. Trugman, J. F. O’Hara, and A. J. Taylor (2008). “Electronic control of extraordinary terahertz transmission through subwavelength metal hole arrays,” *Opt.Express* 16(11), 7641–7648.

-
- ✦ Chen Lin, Jiaming Xu, Chunmei Gao, Xiaofei Zang, Bin Cai, and Yiming Zhu (2013). “Manipulating terahertz electromagnetic induced transparency through parallel plate waveguide cavities” *Applied Physics Letters* 103, 251105.
- ✦ Clawson R. (2001). Guide to references on III–V semiconductor chemical etching, *Materials Science and Engineering: R: Reports*, Volume 31, Issues 1–6, Pages 1-438, ISSN 0927-796X, [http://dx.doi.org/10.1016/S0927-796X\(00\)00027-9](http://dx.doi.org/10.1016/S0927-796X(00)00027-9).
- ✦ Cooper E. Donald (1985). “Picosecond optoelectronic measurement of microstrip dispersion.” *Applied Physics Letters* 47, 33.
- ✦ Cunningham P. D., N. N. Valdes, F. A. Vallejo, L. M. Hayden, B. Polishak, X.H. Zhou, J. Luo, A. K.Y. Jen, J. C. Williams, and R. J. Twieg (2011). “Broadband terahertz characterization of the refractive index and absorption of some important polymeric and organic electro-optic materials” *Journal of Applied Physics*, 109, 4, 043505.
- ✦ Dionne J. A., Sweatlock, L. A., Atwater, H. A., Polman, A. (2005). “Planar metal plasmon waveguides: frequency-dependent dispersion, propagation, localization, and loss beyond the free electron model.” *Physical Review B*, 72 (7).
- ✦ Dionne J. A., Sweatlock, L. A., Atwater, H. A., Polman, A. (2006). “Plasmon slot waveguides: Towards chip-scale propagation with subwavelength-scale localization” *Phys. Rev. B* 73, 035407.
- ✦ Dragoman M and Dragoman D. (2008), “Plasmonics: Applications to nanoscale terahertz and optical devices.” *Progress in Quantum Electronics*, vol. 32, no. 1, pp. 1–41.
- ✦ Ebbesen T. W, Lezec H.J, Ghaemi H.F, Thio T and Wolff P.A (1998). “Extraordinary optical transmission through sub-wavelength hole arrays”. *Nature* 391, 667.
- ✦ Ebbesen T. W., Degiron A, Devaux E, Linke RA, Martin-Moreno L, Garcia-Vidal FJ, . (2002) “Beaming light from a subwavelength aperture” *Science*. 297 (5582):820-822.
- ✦ Exter M. van, and D. Grischkowsky (1990) “Carrier dynamics of electrons and holes in moderately doped silicon,” *Phys. Rev. B* 41(17), 12140–12149.
- ✦ Fattinger Ch. and Grischkowsky D. (1988). “Point source terahertz optics.” *Applied Physics Letters*, 53, 1480-1482.
- ✦ Gallant, A. J. and Kaliteevski, M. A. and Brand, S. and Wood, D. and Petty, M. and Abram, R. A. and Chamberlain, J. M. (2007). “Terahertz frequency bandpass filters.”
-

-
- Journal of Applied Physics*, 102, 023102
- ✦ Gelmont B, Parthasarathy R, Globus T, Bykhovski A, Swami N. (2008), “Terahertz (THz) Electromagnetic Field Enhancement in Periodic Subwavelength Structures”, *Sensors Journal, IEEE* , vol.8, no.6, pp.791,796.
 - ✦ Grigorenko A. N., Polini M. and Novoselov K. S. (2012), “Graphene plasmonics.” *Nature Photonics*, 6,749–758.
 - ✦ Grischkowsky D. (2000) "Optoelectronic characterization of transmission lines and waveguides by terahertz time-domain spectroscopy," *IEEE Journal of Selected Topics in Quantum Electronics*, vol.6, no.6, pp.1122,1135. doi: 10.1109/2944.902161.
 - ✦ Hasebe, S. Kawabe, H. Matsui, and H. Tabata (2012). “Metallic mesh-based terahertz biosensing of single- and double-stranded DNA,” *J. Appl. Phys*, 112, 094702.
 - ✦ Heinz Raether (1988). “Surface Plasmons on smooth and rough surfaces on Gratings.” *Springer-Verlag Tracts in Modern Physics*, volume 111 New York.
 - ✦ Hendry E., F. J. Garcia-Vidal, L. Martin-Moreno, J. Gómez Rivas, M. Bonn, A. P. Hibbins, and M. J. Lockyear (2008). “Optical control over surface plasmon polariton-assisted THz transmission through a slit aperture,” *Phys. Rev. Lett.* 100(12), 123901
 - ✦ Hocker G. B. and Burns W. K. (1977). “Mode dispersion in diffused channel waveguides by the effective index method.” *Appl. Opt.* 16, 113-118.
 - ✦ Isaac T. H., Rivas J. Gómez, Sambles J. R., Barnes W. L., and Hendry E. (2008). “Surface plasmon mediated transmission of subwavelength slits at THz frequencies” *Phys. Rev. B* 77, 113411.
 - ✦ Jin Tao, Bin Hu, Xiao Yong He, Qi Jie Wang (2013). “Tunable Subwavelength Terahertz Plasmonic Stub Waveguide Filters” *IEEE Transactions on Nanotechnology*, 12, 6, 1191-1197.
 - ✦ John F. O'Hara, Ranjan Singh, Igal Brener, Evgenya Smirnova, Jianguang Han, Antoinette J. Taylor, and Weili Zhang, (2008). "Thin-film sensing with planar terahertz metamaterials: sensitivity and limitations," *Optics. Express* 16, 1786-1795.
 - ✦ Keiser G. (1991). *Optical Fiber Communications*, McGraw-Hill, 1991.
 - ✦ Kimberly S. Reichel, Krzysztof Iwaszczuk, Peter U. Jepsen, Rajind Mendis, and Daniel M. Mittleman (2014). “In situ spectroscopic characterization of a terahertz resonant cavity”, *Optica* 1, 272-275.
 - ✦ Kitagawa, J. and Ohkubo, T. and Onuma, M. and Kadoya Y. (2006). “THz spectroscopic characterization of biomolecule/water systems by compact sensor chips.” *Appl. Phys. Lett.* **89**, 041114.
-

-
- ✦ Knox R.M. and P.P. Toullos (1970). “Integrated circuits for millimetre through optical frequency range.” Edited Fox J., Ed., Proc. MRI Symposium on sub millimetre waves, Brooklyn 497-516.
- ✦ Koichiro Ueno, Edson Gomes Camargo, Takashi Katsumata, Hiromasa Goto, Naohiro Kuze, Yoshihiro Kangawa and Koichi Kakimoto (2013). “InSb Mid-Infrared Photon Detector for Room-Temperature Operation” *Jpn. J. Appl. Phys.* 52 092202 doi:10.7567/JJAP.52.092202.
- ✦ Kretschmann E. and Raether. H (1968). “Radiative Decay of Non Radiative Surface Plasmons Excited by Light.” *Zeit.fur Naturforschung*, 23a, 2135-2136.
- ✦ Kumar G., S. Pandey, A. Cui, and A. Nahata (2011). “Planar plasmonic terahertz waveguides based on periodically corrugated metal films” *New Journal of Physics*, **13**, 3, 033024.
- ✦ Laman. N, S. S. Harsha, D. Grischkowsky, and J. S. Melinger (2008). “High Resolution Waveguide THz Spectroscopy of Biological Molecules”, *Biophysical Journal*, 94, 3, 1010–1020.
- ✦ Lamprecht B., Krenn J.R., Schider G., Ditzbacher H., Salerno M., Felidj N., Leitner A., Aussenegg F. R., Weeber J.C. (2001). “Surface plasmon propagation in microscale metal stripe.” *Applied Physics Letters*, Vol. 79, No. 1.
- ✦ Lo Shu-Zee A. and Murphy Thomas E (2010), “Terahertz surface plasmon propagation in nanoporous silicon layers”, *Applied Physics Letters*, 96, 201104.
- ✦ Longqing Cong, Siyu Tan, Riad Yahiaoui, Fengping Yan, Weili Zhang, and Ranjan Singh (2015). “Experimental demonstration of ultrasensitive sensing with terahertz metamaterial absorbers: A comparison with the metasurfaces.” *Appl. Phy Letts*, 106, 031107.
- ✦ Marti O., Bielefeldt H., Hecht B., Herminghaus S., Leiderer P., Mlynek J.(1993). “Near-field optical measurement of the surface plasmon field, *Optics Communications*.” Volume 96, Issues 4–6, 15 Pages 225-228.
- ✦ Markelz A.G., A Roitberg, E.J Heilweil (2000). “Pulsed terahertz spectroscopy of DNA, bovine serum albumin and collagen between 0.1 and 2.0 THz” *Chemical Physics Letters*, 320, 1–2, 31.
- ✦ Matsuzaki, T. Okamoto, M. Haraguchi, M. Fukui, and M. Nakagaki (2008). “Characteristics of gap plasmon waveguide with stub structures,” *Opt. Express* 16, 16314-16325.
-

-
- ♣ Masayoshi Tonouchi (2007). “Cutting-edge terahertz technology.” *Nature Photonics* 1, 97 – 105.
- ♣ McGowan R. W. and Grischkowsky D. (1999). “Experimental time-domain study of THz signals from impulse excitation of a horizontal surface dipole.” *Applied Physics Letters*, 74, 1764-1766 (1999)
- ♣ Mendis R, V. Astley, J. Liu, and D. M. Mittleman (2009), “Terahertz microfluidic sensor based on a parallel-plate waveguide resonant cavity”, *Applied Physics Letters*, vol. 95, no. 17, p. 171113.
- ♣ Nagel M., Haring Bolivar P., M. Brucherseifer, H. Kurz, A. Bosserhoff, and R. Büttner (2002). “Integrated THz technology for label-free genetic diagnostics.” *Appl. Phys. Lett.* 80(1), 154– 156.
- ♣ Pannipitiya Asanka, Rukhlenko D. Ivan, Premaratne Malin, Hattori T. Haroldo, and Agrawal P. Govind P. (2010). “Improved transmission model for metal-dielectric-metal plasmonic waveguides with stub structure.” *Optics Express* 18, 6191-6204.
- ♣ Paul A. George, Christina Manolatu, Farhan Rana. Adam L. Bingham and Daniel R. Grischkowsky (2007). “Integrated waveguide-coupled terahertz microcavity resonators.” *Appl. Phys. Lett.* , 91, 191122.
- ♣ Paul A. George, Wallace Hui, Farhan Rana, Benjamin G. Hawkins, A. Ezekiel Smith, Brian J. Kirby (2008). “Microfluidic devices for terahertz spectroscopy of biomolecules.” *Optics Express*, 16, 3, 16314-16325.
- ♣ Paul Drude (1900). “Zur Elektronentheorie der metalle.”. *Annals of Physics*, 1, 566-613.
- ♣ Pendry J (2000). “Negative Refraction Makes a Perfect Lens.” *Physical Review Letter.* 85, 39663969.
- ♣ Pendry J., Krishnan, T Thio, T.J Kim, H.J Lezec, T.W Ebbesen, P.A Wolff, L Martin-Moreno, F.J Garcia-Vidal (2001). “Evanescently coupled resonance in surface plasmon enhanced transmission. *Optics Communications*, Volume 200, Issues 1–6, Pages 1-7.
- ♣ Pozar D. M, *Microwave Engineering*, 2nd ed. (Wiley, New York, 1998).
- ♣ Prade B., Vinet J. Y., Mysyrowicz A. (1991). “Guided optical waves in planar heterostructures with negative dielectric constant.” *Phys. Rev. B* 44, 13556–13572.
- ♣ Reichel K., Iwaszczuk K., Jepsen P., Mendis R., and D. Mittleman (2014), “In situ spectroscopic characterization of a terahertz resonant cavity” *Optica* 1, 272-275.
- ♣ Ritchie (1957). “Plasma Losses by Fast Electrons in Thin Films.” *Phy.Rev.*, 106(5), 874-881.
-

-
- ✦ Rivas J. G, P. H. Bolivar, and H. Kurz (2004), “Thermal switching of the enhanced transmission of terahertz radiation through sub-wavelength apertures,” *Opt. Lett.* 29(14), 1680–1682.
- ✦ Sambles R., Bradbery G. W and Fuzi Yang (1991). “Optical excitation of surface plasmons: An introduction.” *Contemporary Physics* Volume 32, Issue 3, pages 173-183
- ✦ Singh Ranjan, Wei Cao, Ibraheem Al-Naib, Longqing Cong, Withawat Withayachumnankul, and Weili Zhang (2014). “Ultrasensitive terahertz sensing with high-Q Fano resonances in metasurfaces”, *Applied Physics Letters*, 105,171101.
- ✦ Sommerfeld A. (1899), “Ueber die Fortpflanzung elektrodynamischer Wellen langs eines Drahtes.” *Ann. Phys. U. Chem.*, 67, 233-290.
- ✦ Stefan A Maier (2006). ‘Plasmonics: Fundamentals and Applications.’ *Springer-verlag*, New York.
- ✦ Stefan A Maier (2012). “Graphene plasmonics: All eyes on flatland.” *Nature Physics* 8, 581–582
- ✦ Steven R Andrews (2014) “Microstructured terahertz waveguides” *J. Phys. D: Appl. Phys.* 47 374004. doi:10.1088/0022-3727/47/37/374004
- ✦ Takahara J., Yamagishi S., Taki H., Morimoto A., Kobayashi T.(1997). “Guiding of a one-dimensional optical beam with nanometer diameter” *Optics Letter* 22, 475477.
- ✦ Tournois Pierre, Laude Vincent (1997). “Negative group velocities in metal-film optical waveguides, *Optics Communications.*” Volume 137, Issues 1–3, 15, Pages 41-45.
- ✦ Vakil, A., Engheta, N. (2011). “Transformation Optics Using Graphene.” *Science* 332, 1291–1294.
- ✦ Veronis G. and Shanhui Fan (2005), “Bends and splitters in metal-dielectric-metal subwavelength plasmonic waveguides,” *Appl. Phys. Lett.* 87, 131102(1-3).
- ✦ Veronis, G. Shanhui Fan (2007). “Modes of Subwavelength Plasmonic Slot Waveguides.” *J. Lightwave Technology*, vol.25, no.9, pp.2511-2521.
- ✦ Vincenzo Giannini, Berrier A., Maier S. A., Sánchez-gil J. A., and J. G. Rivas J. A. (2010), “Scattering efficiency and near field enhancement of active semiconductor plasmonic antennas at terahertz frequencies” *Optics Express*, 18, 3, 7028–7034.
- ✦ Wächter Markus, Michael Nagel, and Heinrich Kurz, (2007). “Metallic slit waveguide for dispersion-free low-loss terahertz signal transmission” *Applied Physics Letters* 90, 061111; doi: 10.1063/1.2472544.
-

-
- ♣ Weeber J.C., Krenn J. R., Dereux A., Lamprecht B., Lacroute Y., and Goudonnet J. P (2001). “Near-field observation of surface plasmon polariton propagation on thin metal stripes”, *Phys. Rev. B*, 64, 045411.
 - ♣ Yang Hongyan, Li Jianqing, Xiao Gongli (2014). “A highly efficient surface plasmon polaritons excitation achieved with a metalcoupled metal-insulator-metal waveguide” *AIP Advances* 4, 127114.
 - ♣ You B, J.-Y. Lu, C.-P. Yu, T.-A. Liu, and J.-L. Peng. (2012). “Terahertz refractive index sensors using dielectric pipe waveguides.” *Optics express*, vol. 20, no. 6, pp. 5858–66.
 - ♣ Zenneck J. (1907). “Fortplafanzung ebener elektromagnetischer Wellen lands einer ebenen Leiterflache.”, *Ann. D. Phys.*, 23, 846-866.
 - ♣ Zhan Hui, Rajind Mendis, and Daniel M. Mittleman (2011). “Characterization of the terahertz near-field output of parallel-plate waveguides”, *J. Opt. Soc. Am. B*, 28, 558-566
 - ♣ Zhu X. L., Yan W., Mortensen N. A. & Xiao S. S. (2013). “Bends and splitters in graphene nanoribbon waveguides.” *Optics Express*, 21, 3486–3491.
 - ♣ Zhu. W, A. Agrawal, A. Cui, G. Kumar, and A. Nahata (2011). “Engineering the Propagation Properties of Planar Plasmonic Terahertz Waveguides”, *IEEE Journal of Selected Topics in Quantum Electronics*, vol. 17, no. 1, pp. 146–153.
 - ♣ Zia Rashid, Selker Mark D., Catrysse Peter B., and Brongersma Mark L. (2004). "Geometries and materials for subwavelength surface plasmon modes." *J. Opt. Soc. Am. A* 21, 2442-2446.
 - ♣ Zheng Jiajiu, Longhai Yu, Sailing He Daoxin Dai (2015). “Tunable pattern-free graphene nanoplasmonic waveguides on trenched silicon substrate”, *Scientific Reports* 5, Article No. 7987, doi:10.1038/srep07987.

LIST OF PUBLICATIONS

(A) Research papers in International Journals

- 1 **Shourie Ranjana J**, Piyush Bhatt, Harshad Surdi, Bagvanth Sangala, M.N, Satyanarayan, G, Umesh, S S, Prabhu (2016), “Resonant Terahertz InSb Plasmonic Waveguide Device for Sensing Polymers ” – Journal of Infrared Millimeter and Terahertz wave, Springer Publications 10.1007/s10762-016-0268-7.
- 2 **Shourie Ranjana J**, Piyush Bhatt, Harshad Surdi, Bagvanth Sangala, M.N, Satyanarayan, G, Umesh, S S, Prabhu (2015), “Bio-interfacing of resonant transmission characteristics of InSb based Terahertz Plasmonic waveguide” – Biomed. Phys. Eng. Express 1 025003 doi:10.1088/2057-1976/1/2/025003

(B) Research papers in International conferences

- 1 **Shourie Ranjana J**, Bhatt P, Surdi H, Sangala B.R, Satyanarayan M.N, Umesh G, Prabhu S.S (2015), "Indium Antimonide (InSb) waveguide based THz sensor," 2015 IRMMW, University of Hong Kong, IEEE Conf. Proceedings. 10.1109/IRMMW-THz.2015.7327917.
- 2 **Shourie Ranjana J**, Bhatt P, Surdi H, Sangala B.R, Satyanarayan M.N, Umesh G, Prabhu S.S (2014), "Indium Antimonide (InSb) based planar terahertz plasmonic waveguide," IEEE Conf. Proc, DOI: 10.1109/IRMMW-THz.2014.6956437
- 3 **Shourie Ranjana J**, M. N. Satyanarayan and G. Umesh (2013). Indium Antimonide (InSb) Cavity Resonators based on Planar Plasmonic Terahertz Waveguide. MRS Proceedings, 1566, mrss13-1566-ii09-19 DOI:10.1557/opl.2013.944.
- 4 **Shourie Ranjana J.**, M. N. Satyanarayan, G. Umesh, (2014). “Indium Antimonide (InSb) based Planar Terahertz Plasmonic Cavity Resonator as Biosensors” 2014 International Conference of Optics and Optoelectronics, XXXVIII Symposium of optical society of India. 5th March to 8th March 2014, Dehradun, Uttarkhand, INDIA.
- 5 **Shourie Ranjana J**, M. N. Satyanarayan, G. Umesh, (2011). “Surface Plasmon Propagation on Metal Insulator Metal (MIM) waveguide: Simulation Studies”, Recent Trends in Nanophotonics” 30th Sep to 1st Oct 2011, IIT Delhi, INDIA.

17, Chinnasamy Pillai Street, Bethaniapuram

Madurai – 625016, Tamilnadu

India

Ph: 09008909165

shourieranjana@gmail.com

SHOURIE RANJANA J

EDUCATION

⊙ **Ph.D in Physics (THz Plasmonics)**

Title: “Investigations on InSb plasmonic devices for sensor applications at Terahertz frequencies”

Institute: NITK Surathkal, Mangalore, INDIA.

Advisor: Prof. G. Umesh and Dr. M.N. Satyanarayan

Year: Thesis submitted (October 2015)

⊙ **M.Sc. Physics** [2008 - 10]

NITK Surathkal, Mangalore, INDIA.

⊙ **B.Sc. Physics** [2005 - 08]

Madurai Kamarajar University, Lady Doak College, Madurai, INDIA.

HIGHLIGHTS

- ❖ Excellent academic record (CP1 ~8.5/10)
 - ❖ Expertise in performing electromagnetic simulations.
 - ❖ Expertise in simulation, fabrication and characterization of Terahertz (THz) and optical waveguide, resonators and filter at, NITK Surathkal, IITBNF in IIT Bombay and TIFR Mumbai.
-

RESEARCH INTEREST

- ❖ Novel electromagnetic devices for future technology
 - ❖ Fabricate and characterize integrated electromagnetic devices with lab on chip environment.
 - ❖ New materials for electromagnetic device applications.
-

RESEARCH EXPERTISE

THz planar plasmonic Indium Antimonide (InSb) waveguides (PhD).

- ❖ Design and Simulate THz plasmonic waveguide using COMSOL[®] Multiphysics as a resonant structure using InSb. Including modelling the frequency dependent property of InSb.
- ❖ Fabrication of InSb pellets and laser micromachining of InSb THz waveguides.
- ❖ Characterization of InSb waveguide using standard terahertz time domain spectroscopy in transmission mode (THz-TDS) in determining the resonant nature of the device.
- ❖ Testing the InSb waveguide with bio chemical samples like proteins, blood serum and polymer to monitor its function as a sensitive chemical sensor.

Fabrication of SU8 based multimode optical waveguides and ring resonators (MSc).

- ❖ Design and simulate SU8 based optical waveguide and ring resonators using RSOFT Beamprob for multimode operation.
- ❖ Fabricate waveguide and resonators using spin coating and basic lithography technique in semi clean room environment.

Third order nonlinear optical studies of polymer doped organic molecules(MSc).

- ❖ Fabricate PMMA doped with third order nonlinear organic molecule, thin films using spin coating technique on glass substrates.
- ❖ Characterize the thin films using Z-Scan technique and study the optical limiting property of the films.

TECHNICAL SKILLS

Developed technical expertise in simulation and fabrication of THz devices during my PhD through working in NITK Surathkal, Nanofabrication lab in IIT Bombay and TIFR, Mumbai

- ❖ **Simulation Skills:** RF simulation in COMSOL[®] Multiphysics, Ansoft HFSS, CST Microwave Studio, BeamProb Rsoft, MEEP- FDTD.
- ❖ **Fabrication Skills:** Laser ablation and micromachining using ND: YAG laser, Thermal evaporation, Pulsed laser deposition, Spin coating technique, Basic optical lithography.
- ❖ **Characterization Skill:** THz TDS, Z-Scan, UV absorption spectroscopy, Electrical characterization (IV, CV) using Cascade Probe station.
- ❖ Expertise in designing, setting up and handling optical and THz measurements.

- ❖ Expertise in writing of scientific and technical papers and documentations.
-

WORK EXPERIENCE

- ❖ Teaching Assistant in Department of Physics, NITK – Teaching different courses on Electromagnetic theory and Engineering Physics at under graduate and post graduate level (July 2010 – present)
-

LIST OF PUBLICATIONS

- 1 **Shourie Ranjana J**, Piyush Bhatt, Harshad Surdi, Bagvanth Sangala, M.N, Satyanarayan, G, Umesh, S S, Prabhu (2016), “Resonant Terahertz InSb Plasmonic Waveguide Device for Sensing Polymers ” – Journal of Infrared Millimeter and Terahertz wave, Springer Publications 10.1007/s10762-016-0268-7.
- 2 **Shourie Ranjana J**, Piyush Bhatt, Harshad Surdi, Bagvanth Sangala, M.N, Satyanarayan, G, Umesh, S S, Prabhu (2015), “Bio-interfacing of resonant transmission characteristics of InSb based Terahertz Plasmonic waveguide” – Biomed. Phys. Eng. Express 1 025003 doi:10.1088/2057-1976/1/2/025003

CONFERENCE PROCEEDINGS

- 1 **Shourie Ranjana J**, Bhatt P, Surdi H, Sangala B.R, Satyanarayan M.N, Umesh G, Prabhu S.S (2015), "Indium Antimonide (InSb) waveguide based THz sensor," 2015 IRMMW, University of Hong Kong, IEEE Conf. Proceedings. 10.1109/IRMMW-THz.2015.7327917
 - 2 **Shourie Ranjana J**, Bhatt P, Surdi H, Sangala B.R, Satyanarayan M.N, Umesh G, Prabhu S.S (2014), "Indium Antimonide (InSb) based planar terahertz plasmonic waveguide," IEEE Conf. Proc, DOI: 10.1109/IRMMW-THz.2014.6956437
 - 3 **Shourie Ranjana J**, M. N. Satyanarayan and G. Umesh (2013). Indium Antimonide (InSb) Cavity Resonators based on Planar Plasmonic Terahertz Waveguide. MRS Proceedings, 1566, mrs13-1566-ii09-19 DOI:10.1557/opl.2013.944.
 - 4 **Shourie Ranjana J**, M. N. Satyanarayan, G. Umesh, (2014). “Indium Antimonide (InSb) based Planar Terahertz Plasmonic Cavity Resonator as Biosensors” 2014 International Conference of Optics and Optoelectronics, XXXVIII Symposium of optical society of India. 5th March to 8th March 2014, Dehradun, Uttarkhand, INDIA.
 - 5 **Shourie Ranjana J**, M. N. Satyanarayan, G. Umesh, (2011). “Surface Plasmon Propagation on Metal Insulator Metal (MIM) waveguide: Simulation Studies”, Recent Trends in Nanophotonics” 30th Sep to 1st Oct 2011, IIT Delhi, INDIA.
-

AWARDS

- ❖ National award for First prize in Indian National Physics talent quest 2008 organized by Indian Physics association, Mumbai.
-

REFERENCES

Prof. G. Umesh, umesh52@gmail.com, Department of Physics, NITK Surathkal

Dr. M. N. Satyanarayan, mn.satyanarayan@gmail.com, Department of Physics, NITK Surathkal

Prof. S. S. Prabhu, shriganesh.prabhu@gmail.com, DCMPMS, TIFR, Mumbai

PERSONAL DETAILS

Date of birth : 2nd July 1987

Gender : Female

Father's Name : Jebamalaidass A.

Mother's Name : Maria Madalene A.

Nationality : Indian

Mother tongue : Tamil

Home Town : Madurai, Tamilnadu, INDIA

Language known : English, Tamil, Kannada

DECLARATION

I hereby declare that the details furnished above are true and unbiased to the best of my knowledge.

SHOURIE RANJANA J.

Place: Surathkal, Karnataka